A series of energetic eruptions leading to a peculiar H-rich explosion of a massive star

Iair Arcavi[1,2,3,4], D. Andrew Howell[1,3], Daniel Kasen[5,7,8], Lars Bildsten[2,3], Griffin Hosseinzadeh[1,3], Curtis McCully[1,3], Zheng Chuen Wong[1,3], Sarah Rebekah Katz[1,3], Avishay Gal-Yam[9], Jesper Sollerman[10], Francesco Taddia[10], Giorgos Leloudas[9,11], Christoffer Fremling[10], Peter E. Nugent[6,8], Assaf Horesh[12,9], Kunal Mooley[13], Clare Rumsey[14], S. Bradley Cenko[15,16], Melissa L. Graham[17,7,8], Daniel A. Perley[11], Ehud Nakar[18], Nir J. Shaviv[12], Omer Bromberg[18], Ken J. Shen[7,8], Eran O. Ofek[9], Yi Cao[19], Xiaofeng Wang[20], Fang Huang[20], Liming Rui[20], Tianmeng Zhang[21], Wenxiong Li[20], Zhitong Li[20], Jujia Zhang[22,23], Stefano Valenti[24], David Guevel[1,3], Benjamin Shappee[25,26], Christopher S. Kochanek[27,28], Thomas W.-S. Holoien[27,28], Alexei V. Filippenko[7,8], Rob Fender[13], Anders Nyholm[10], Ofer Yaron[9], Mansi M. Kasliwal[19], Mark Sullivan[29], Nadja Blagorodnova[19], Richard S. Walters[19], Ragnhild Lunnan[19], Danny Khazov[9], Igor Andreoni[30,31,32], Russ R. Laher[33], Nick Konidaris[34], Przemek Wozniak[35] and Brian Bue[36]

[1] *Las Cumbres Observatory, Goleta, CA 93117, USA*

[2] *Kavli Institute for Theoretical Physics, University of California, Santa Barbara, CA 93106, USA*

[3] *Department of Physics, University of California, Santa Barbara, CA 93106, USA*

[4] *Einstein Fellow*

[5] *Nuclear Science Division, Lawrence Berkeley National Laboratory, Berkeley, CA 94720, USA*

[6] *Computational Research Division, Lawrence Berkeley National Laboratory, Berkeley, CA 94720, USA*

[7] *Department of Physics, University of California, Berkeley, CA 94720, USA*

[8]Department of Astronomy, University of California, Berkeley, CA 94720-3411, USA

[9]Department of Particle Physics and Astrophysics, The Weizmann Institute of Science, Rehovot, 76100, Israel

[10]The Oskar Klein Centre, Department of Astronomy, Stockholm University, AlbaNova, SE-10691 Stockholm, Sweden

[11]Dark Cosmology Centre, Niels Bohr Institute, University of Copenhagen, Juliane Maries vej 30, 2100 Copenhagen, Denmark

[12]Racah Institute of Physics, The Hebrew University of Jerusalem, Jerusalem 91904, Israel

[13]Department of Physics, Astrophysics, University of Oxford, Denys Wilkinson Building, Oxford, OX1 3RH, UK

[14]Astrophysics Group, Cavendish Laboratory, 19 J. J. Thomson Avenue, Cambridge, CB3 0HE

[15]Astrophysics Science Division, NASA Goddard Space Flight Center, Code 661, Greenbelt, MD 20771, USA

[16]Joint Space-Science Institute, University of Maryland, College Park, MD 20742, USA

[17]Department of Astronomy, University of Washington, Box 351580, U.W., Seattle, WA 98195-1580

[18]The Raymond and Beverly Sackler School of Physics and Astronomy, Tel Aviv University, Tel Aviv 69978, Israel

[19]Cahill Center for Astrophysics, California Institute of Technology, Pasadena, CA 91125, USA

[20]Physics Department and Tsinghua Center for Astrophysics (THCA), Tsinghua University, Beijing, 100084, China

[21]*National Astronomical Observatories of China, Chinese Academy of Sciences, Beijing, 100012, China*

[22]*Yunnan Observatories, Chinese Academy of Sciences, Kunming 650011, China*

[23]*Key Laboratory for the Structure and Evolution of Celestial Objects, Chinese Academy of Sciences*

[24]*Department of Physics, University of California, 1 Shields Ave, Davis, CA 95616, USA*

[25]*Carnegie Observatories, 813 Santa Barbara Street, Pasadena, CA 91101, USA*

[26]*Hubble Fellow, Carnegie-Princeton Fellow*

[27]*Department of Astronomy, The Ohio State University, 140 West 18th Avenue, Columbus, OH 43210, USA*

[28]*Center for Cosmology and AstroParticle Physics (CCAPP), The Ohio State University, 191 W. Woodruff Ave., Columbus, OH 43210, USA*

[29]*Department of Physics and Astronomy, University of Southampton, Southampton SO17 1BJ, UK*

[30]*Centre for Astrophysics and Supercomputing, Swinburne University of Technology, PO Box 218, VIC 3122, Australia*

[31]*ARC Centre of Excellence for All-sky Astrophysics (CAASTRO)*

[32]*Australian Astronomical Observatory, PO Box 915, North Ryde, NSW 1670, Australia*

[33]*Spitzer Science Center, California Institute of Technology, MS 314-6, Pasadena, CA 91125, USA*

[34]*Kairos Aerospace, 777 Cuesta Drive, Suite 202, Mountain View, CA, 94040*

[35]*Space and Atmospheric Sciences Group, Mail Stop D466, Los Alamos National Laboratory, Los*

Alamos, NM 87545

[36] *Jet Propulsion Laboratory, California Institute of Technology, Pasadena, CA 91109, USA*

Every supernova hitherto observed has been the terminal explosion of a star. And all supernovae with absorption lines in their spectra show those lines decreasing in velocity over time, as the ejecta expands and thins, revealing slower moving material that was previously hidden. In addition, every supernova that shows absorption lines of hydrogen has one main lightcurve peak, or a plateau in luminosity for approximately 100 days before declining[1]. Here we report observations of iPTF14hls, an event that has spectra identical to a hydrogen-rich core-collapse supernova, but which violates all of the above supernova principles: The lightcurve has at least five peaks and stays bright for more than 600 days; The absorption lines show little to no decrease in velocity; The radius of the line-forming region is more than an order of magnitude bigger than the radius of the photosphere derived from the continuum emission. This is consistent with a shell of a few 10's of solar masses ejected by the star at supernova-level energies a few hundred days prior to a terminal explosion. Another possible eruption was recorded at the same position in 1954. Multiple energetic pre-supernova eruptions are expected to occur in ≈95–130 solar mass stars which experience the pulsational pair instability[2, 3, 4, 5]. However, that scenario does not account for the continued presence of hydrogen nor the energetics observed here, prompting the need for a new violent mass ejection mechanism for massive stars.

On 2014 Sep. 22.53 (UT dates are used throughout), the iPTF survey[6, 7] discovered iPTF14hls at right ascension, $\alpha_{\rm J2000} = 09{\rm h}\ 20{\rm m}\ 34.30{\rm s}$ and declination, $\delta_{\rm J2000} = +50^\circ 41' 46.8''$, at an R-band magnitude of 17.716 ± 0.033 (Extended Data Fig. 1). We have no observations of this position between 2014 May 28 and Sep 22, inducing a ≈100-day uncertainty in the explosion time, so we use the discovery date as a reference epoch for all phases. We adopt a redshift of $z = 0.0344$, determined from narrow host-galaxy features, corresponding to a luminosity distance of 156 Mpc[9].

On 2015 Jan. 8, iPTF14hls was classified as a Type II-P supernova based on prominent broad Balmer series P-Cygni lines in an optical spectrum[8]. So far, Type II-P supernovae have been the only events ever observed to produce such spectra. In a Type II-P, the core of a massive star collapses to create a neutron star, sending a shock through the outer hydrogen-rich envelope, ejecting it. The shock ionizes the ejecta, which later expand, cool and recombine. The photosphere follows the recombination front, which is at a roughly constant temperature ($T \approx 6000\,\mathrm{K}$) as it makes its way inward in mass through the expanding ejecta[10]. This leads to the ≈100-day "plateau" phase of roughly constant luminosity in the light curve and prominent hydrogen P-Cygni features in the spectrum.

iPTF14hls, while identical to Type II-P supernovae in its spectroscopic features, has several properties never before seen in a supernova. Instead of a 100-day plateau, the light curve of iPTF14hls lasts over 600 days and has at least five distinct peaks during which the luminosity varies by as much as $\approx 50\%$ (Fig. 1). Blackbody fits to the broad-band optical *BVgi* photometry of iPTF14hls (see Methods) indicate a roughly constant effective temperature of 5000–6000 K, the same as the hydrogen-recombination temperature typically seen in Type II-P supernovae. However, the inferred bolometric luminosity of a few$\times 10^{42}\,\mathrm{erg\,s^{-1}}$ is on the high end of typical Type II-P supernovae[11], and the total radiated energy of $2.20^{+0.03}_{-0.05} \times 10^{50}$ erg emitted during the 450 days of our multi-band optical coverage is a few times larger than that of any known Type II-P supernova.

Given the uncertainty in explosion time of iPTF14hls, the discrepancies with Type II-P supernova timescales and energetics may be even larger.

The spectroscopic evolution of iPTF14hls is even harder to understand. It is a factor of $\approx$10 slower than that of Type II-P supernovae (Fig. 2); e.g. the spectrum of iPTF14hls at 600 days looks like a normal SN II-P at 60 days (Extended Data Fig. 4). In all previously observed supernovae, the faster material is outside — spectra show a decrease of all measured velocities with time (by a factor of $\approx$3 over 100 days) as the material expands, thins, and the photosphere moves inward in mass revealing deeper, slower-moving material. In iPTF14hls, velocities of hydrogen decline by only 25%, from 8000 km s^{-1} to 6000 km s^{-1} over 600 days, while iron lines stay at a constant velocity of 4000 km s^{-1} (Fig. 3).

It is normal to see hydrogen lines at higher velocity than iron lines due to optical depth effects. But in time, as the material expands and thins, hydrogen should be seen at lower velocity where the iron was previously seen (Extended Data Figure 7). If the ejecta is expanding in size by a factor of $\approx$6 from day 100 to day 600, in the absence of an additional energy source, an inward-moving photosphere scanning through the ejecta in velocity must occur.

An observation of constant velocity can thus be caused by: (1) a central-engine pushing material from the inside, sweeping the ejecta into a thin dense shell[12, 13], or (2) the lines being far above the photosphere, detached from it. One dimensional central-engine models compress the iron and hydrogen lines to the same velocity, which is not the case for iPTF14hls (though multi-dimensional effects could alter this prediction). The line evolution can more readily be explained if the lines are formed by ejecta from a prior eruption that happened a few years before the discovery of iPTF14hls and are detached from the continuum, which was formed in the terminal explosion (see Methods).

We estimate the position of the line-forming region as vt, where v is the observed expansion velocity of the material at time t. For Type II-P supernovae, this radius, when using the iron line velocities, is the same as the photospheric radius obtained by blackbody fits to the continuum emission, up to an order-unity "blackbody dilution factor"[14, 15, 16]. For iPTF14hls, the vt-inferred radius is instead larger than the blackbody-inferred radius by an order of magnitude on day 600 (Fig. 4). The fact that the two radii are so different from each other indicates that the line-forming region in iPTF14hls is indeed spatially detached from the continuum-emitting photosphere, in contrast to what is observed in all known Type II-P supernovae.

The observations are thus consistent with the line-forming material being ejected in a massive and very energetic pre-supernova outburst, specifically in a shell on the order of a few tens of solar masses (see Methods). However, this requires a kinetic energy of $\approx 10^{52}$ erg, normally associated with a supernova. Further evidence for a third even earlier explosion comes from an $M_R \approx -15.6$ magnitude outburst detected at the position of iPTF14hls in 1954 (formally a 2.2σ detection, though this is likely an underestimate due to photographic nonlinearity; see Methods).

Another question is what is powering the light curve of iPTF14hls. Strong asymmetry may induce a luminosity increase in a particular direction. However, we do not detect any significant polarization which would be indicative of asymmetry in the explosion (see Methods). An additional energy source in iPTF14hls compared to normal II-P events could come from the interaction of the ejecta with previously ejected shells. However, in cases of SNe interacting with dense circumstellar material, the interaction dominates the spectra in the form of a strong continuum together with broad, intermediate and narrow components of the Balmer series emission lines[17,18]. None of these features are seen in the spectra of iPTF14hls (Fig. 2; Extended Data Fig. 5). We find no evidence of X-ray or radio emission (which are possible additional indicators of strong interaction)[19] in observations taken during the brightest peak of the optical light curve (see Methods). It is possible any signs of interaction are being reprocessed by overlying, previously ejected material.

Either way, the progenitor of iPTF14hls likely experienced multiple energetic eruptions over the last decades of its life. Energetic eruptions are expected in stars with initial masses of $\approx$95–130 $\mathrm{M}_{\odot}$ (where $\mathrm{M}_{\odot}$ is the solar mass) which undergo an instability arising from the production of electron-positron pairs[2]. Interaction between the different shells and/or the supernova ejecta and the shells can produce a variety of luminous long-lived transients with highly structured light curves[4,5] similar to that of iPTF14hls. Such pulsational-pair instability supernovae are expected to occur in low metallicity environments. iPTF14hls occurred in the outskirts of a low-mass star-forming galaxy, possibly of low metal content (see Methods).

However, models of stars undergoing the pulsational pair instability eject most of the hydrogen envelope in the first eruption[5], whereas for iPTF14hls a few tens of solar masses of hydrogen were retained in the envelope after the 1954 outburst. Another problem is that pulsational pair instability models can account for up to $\sim 4 \times 10^{51}$ erg of kinetic energy in all eruptions together, while $\sim 10^{52}$ erg are required just for the most recent eruption that ejected the line-forming region of iPTF14hls (see Methods).

iPTF14hls demonstrates that stars in the local Universe can undergo very massive eruptions in the decades leading to their collapse yet, surprisingly, maintain a massive hydrogen-rich envelope for most of this period. Current models of massive star evolution and explosion need to be modified, or a completely new picture needs to be put forward, to account for the energetics of iPTF14hls, the lack of strong interaction signatures and the inferred amount of hydrogen it retained towards the end of its life.

1. Arcavi, I. Hydrogen-Rich Core-Collapse Supernovae. In *Handbook of Supernovae*, 1–38 (Springer International Publishing, Cham, 2016). URL `http://link.springer.com/10.1007/978-3-319-20794-0{_}39-1`.

2. Barkat, Z., Rakavy, G. & Sack, N. Dynamics of Supernova Explosion Resulting from Pair Formation. *Physical Review Letters* **18**, 379–381 (1967). URL `http://link.aps.org/doi/10.1103/PhysRevLett.18.379`.

3. Heger, A. & Woosley, S. E. The Nucleosynthetic Signature of Population III. *The Astrophysical Journal, Volume 567, Issue 1, pp. 532-543.* **567**, 532–543 (2002). URL `http://arxiv.org/abs/astro-ph/0107037http://dx.doi.org/10.1086/338487`. 0107037.

4. Woosley, S. E., Blinnikov, S. & Heger, A. Pulsational pair instability as an explanation

for the most luminous supernovae. *Nature, Volume 450, Issue 7168, pp. 390-392 (2007).* **450**, 390–392 (2007). URL http://arxiv.org/abs/0710.3314http://dx.doi.org/10.1038/nature06333. 0710.3314.

5. Woosley, S. E. Pulsational Pair-instability Supernovae. *The Astrophysical Journal* **836**, 244 (2017). URL http://stacks.iop.org/0004-637X/836/i=2/a=244?key=crossref.26431d83a9818abda1d8363b62462c1e.

6. Law, N. M. *et al.* The Palomar Transient Factory: System Overview, Performance and First Results. *Publications of the Astronomical Society of the Pacific* **121**, 1395–1408 (2009). URL http://arxiv.org/abs/0906.5350http://dx.doi.org/10.1086/648598. 0906.5350.

7. Rau, A. *et al.* Exploring the Optical Transient Sky with the Palomar Transient Factory. *Publications of the Astronomical Society of the Pacific* **121**, 1334–1351 (2009). URL http://arxiv.org/abs/0906.5355http://dx.doi.org/10.1086/605911. 0906.5355.

8. Li, W., Wang, X. & Zhang, T. Spectroscopic Classification of CSS141118:092034+504148 as a Type II-P Supernova. *The Astronomer's Telegram* **6898** (2015).

9. Planck Collaboration *et al.* Planck 2015 results. XIII. Cosmological parameters (2015). 1502.01589.

10. Popov, D. V. An analytical model for the plateau stage of Type II supernovae. *The Astrophysical Journal* **414**, 712 (1993). URL http://adsabs.harvard.edu/doi/10.1086/173117.

11. Bersten, M. C. & Hamuy, M. Bolometric Light Curves For 33 Type II Plateau Supernovae. *The Astrophysical Journal* **701**, 200–208 (2009). URL http://adsabs.harvard.edu/abs/2009ApJ...701..200B.

12. Kasen, D. & Bildsten, L. Supernova Light Curves Powered by Young Magnetars. *The Astrophysical Journal* **717**, 245–249 (2010). URL http://adsabs.harvard.edu/abs/2010ApJ...717..245K.

13. Dexter, J. & Kasen, D. Supernova Light Cuves Powered by Fallback Accretion. *The Astrophysical Journal* **772**, 30 (2013). URL http://stacks.iop.org/0004-637X/772/i=1/a=30?key=crossref.6ebc8a4f6831234f803ea155f05e61e2.

14. Kirshner, R. P. & Kwan, J. The envelopes of type II supernovae. *The Astrophysical Journal* **197**, 415 (1975). URL http://adsabs.harvard.edu/abs/1975ApJ...197..415K.

15. Eastman, R. G., Schmidt, B. P. & Kirshner, R. The Atmospheres of Type II Supernovae and the Expanding Photosphere Method. *The Astrophysical Journal* **466**, 911 (1996). URL http://adsabs.harvard.edu/doi/10.1086/177563.

16. Dessart, L. & Hillier, D. J. Distance determinations using type II supernovae and the expanding photosphere method. *Astronomy and Astrophysics* **439**, 671–685 (2005). URL `http://www.edpsciences.org/10.1051/0004-6361:20053217`.

17. Schlegel, . A new subclass of Type II supernovae? *Monthly Notices of the Royal Astronomical Society (ISSN 0035-8711)* **244**, 269–271 (1990). URL `http://adsabs.harvard.edu/abs/1990MNRAS.244..269S`.

18. Kiewe, M. *et al.* Caltech Core-Collapse Project (CCCP) Oobservations of Type IIn Supernovae: Typical Properties and Implications for Their Progenitor Stars. *The Astrophysical Journal* **744**, 10 (2012). URL `http://adsabs.harvard.edu/abs/2012ApJ...744...10K`.

19. Chevalier, R. A., Fransson, C. & Nymark, T. K. Radio and X-Ray Emission as Probes of Type IIP Supernovae and Red Supergiant Mass Loss. *The Astrophysical Journal, Volume 641, Issue 2, pp. 1029-1038.* **641**, 1029–1038 (2006). URL `http://arxiv.org/abs/astro-ph/0509468http://dx.doi.org/10.1086/500528`. `0509468`.

20. Geha, M. *et al.* Variability-Selected Quasars in MACHO Project Magellanic Cloud Fields. *The Astronomical Journal, Volume 125, Issue 1, pp. 1-12.* **125**, 1–12 (2003). URL `http://arxiv.org/abs/astro-ph/0209513http://dx.doi.org/10.1086/344947`. `0209513`.

21. Michel, F. C. Neutron star disk formation from supernova fall-back and possible observational consequences. *Nature* **333**, 644–645 (1988). URL `http://www.nature.com/`

doifinder/10.1038/333644a0.

22. Leonard, D. *et al.* The Distance to SN 1999em in NGC 1637 from the Expanding Photosphere Method. *Publications of the Astronomical Society of the Pacific* **114**, 35–64 (2002). URL http://adsabs.harvard.edu/abs/2002PASP..114...35L.

Competing Interests The authors declare that they have no competing financial interests.

Author Contributions I. Arcavi initiated the study, triggered follow-up observations, reduced data, performed the analysis and wrote the manuscript. DAH is PI of the LCO Supernova Key Project through which all of the LCO data were obtained and assisted with interpretations, and the manuscript. DK and LB assisted with theoretical models, data interpretation and with the manuscript. GH and CM assisted with obtaining and reducing LCO data. ZCW first flagged the supernova as interesting. SRK performed the spectral expansion velocity measurements. AGY is the PI for core-collapse supernovae in iPTF and assisted with interpretations. JS and FT obtained the NOT spectra and polarimetry data and assisted with the manuscript. GL reduced the polarimetry data. CF reduced the P60 data. PEN discovered the 1954 eruption image of iPTF14hls, helped obtain the host-galaxy spectrum, and is a Co-PI on the Keck proposal under which it and one of the supernova spectra were obtained. AH obtained and reduced the VLA data and is PI of the program through which the data were obtained. KM and CR obtained and reduced the AMI data. SBC obtained and reduced the XRT data. MLG obtained and reduced Keck spectra. DAP performed the host-galaxy analysis and assisted with the manuscript. EN, OB, NJS and KJS assisted with theoretical interpretations and with the manuscript. EOO helped with interpretations and the manuscript. YC built the real-time iPTF image-subtraction pipeline and obtained P200 observations. XW, FH, LR, TZ, WL, ZL, and JZ obtained and reduced the Xinglong, Lijiang and TNT data. SV built the LCO photometric and spectroscopic reduction pipelines and assisted with LCO observations, interpretation and the manuscript. DG assisted with the POSS image analysis. BS, CSK, and TW-SH obtained and reduced the ASAS-SN pre-discovery limits. AVF is a Co-PI of the Keck proposal under which the host-galaxy spectrum and one of the supernova spectra were obtained; he also helped with the manuscript. RF is PI of the program through which the AMI data were obtained. AN helped scan for iPTF candidates and assisted with the manuscript. OY is in charge of the iPTF candidate scanning effort. MMK lead the work for building iPTF. MS wrote the pipeline used to reduce P48 data. NB and RSW obtained P60 SEDM photometry. RN, DK, and I. Andreoni obtained P200 observations. RRL contributed to building the P48 image-processing pipeline. NK was a main builder of the P60 SEDM. PW and BB helped build the machine learning algorithms that identify iPTF supernova candidates.

Correspondence Correspondence and requests for materials should be addressed to Iair Arcavi (email: arcavi@gmail.com).

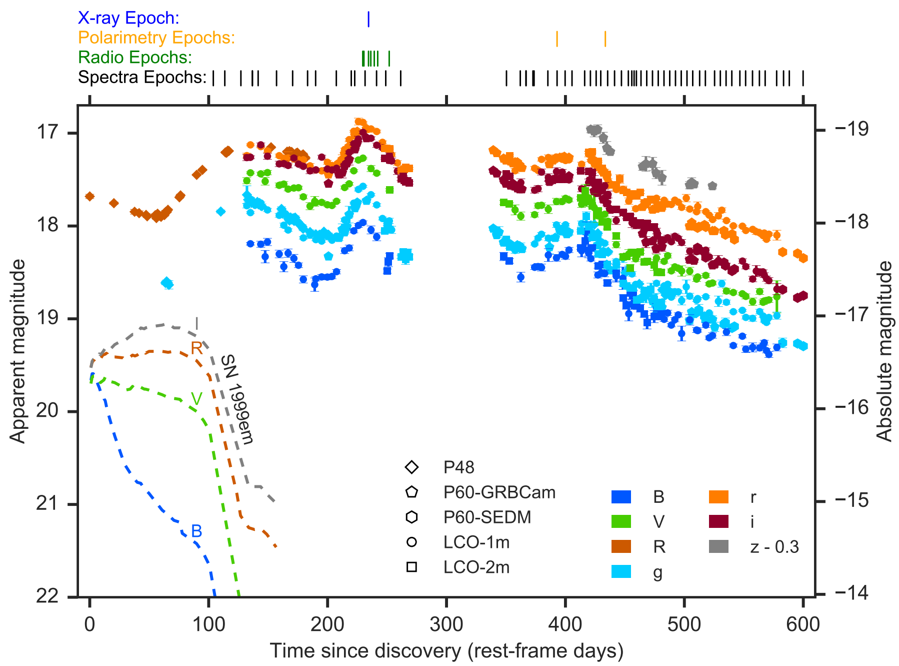

Figure 1 Multi-band optical light curves of iPTF14hls (overlapping data from additional telescopes, not plotted here for clarity, are presented in Extended Data Fig. 2; see Methods for a list of participating telescopes). The prototypical Type II-P SN 1999em is shown for comparison (dashed lines)[22], according to the ordinate axis at right. Photometric points from the same day, instrument, and filter are averaged for clarity. The SEDM i-band data are shifted by $+0.3$ mag to compensate for filter differences with the other instruments. iPTF14hls has at least five distinct peaks in its light curve (at approximately 140, 220, and 410 days after discovery, before discovery as indicated by the R-band light curve, and while the supernova was behind the Sun between days 260 and 340 after discovery). Error bars denote 1σ uncertainties.

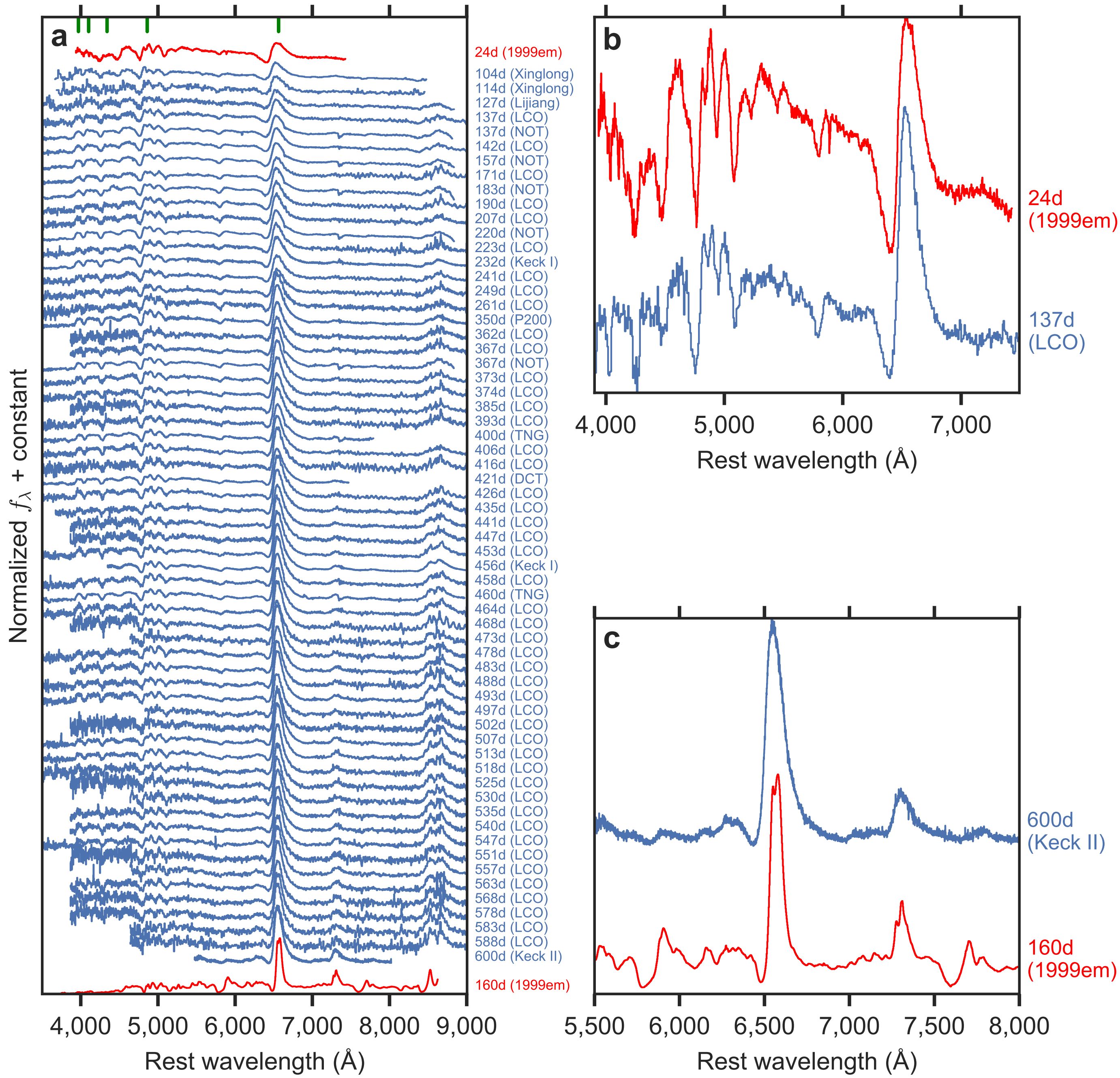

Figure 2 Our full sequence (**a**) of optical spectra of iPTF14hls (blue) with select early-time (**b**) and late-time (**c**) spectra blown up, expressed in terms of normalized flux density

as a function of rest-frame wavelength. The spectra are binned in wavelength and shifted in flux density for clarity. Phases are noted in rest-frame days since discovery on the ordinate axis at right, with the telescope used to obtain the spectrum in parentheses (see Methods for details). Spectra of the prototypical Type II-P SN 1999em[22] (red) are shown for comparison with phases noted in rest-frame days since explosion. Balmer series hydrogen-line wavelengths are denoted in green tick marks at the top of panel (**a**). iPTF14hls is very similar spectroscopically to a normal Type II-P supernova but evolves much more slowly, beginning to become nebular only several hundred days after explosion, yet still showing continuum emission and high velocities even at day 600 (**b**). The spectral evolution is very smooth (**a**), in contrast to the multi-peaked light curve.

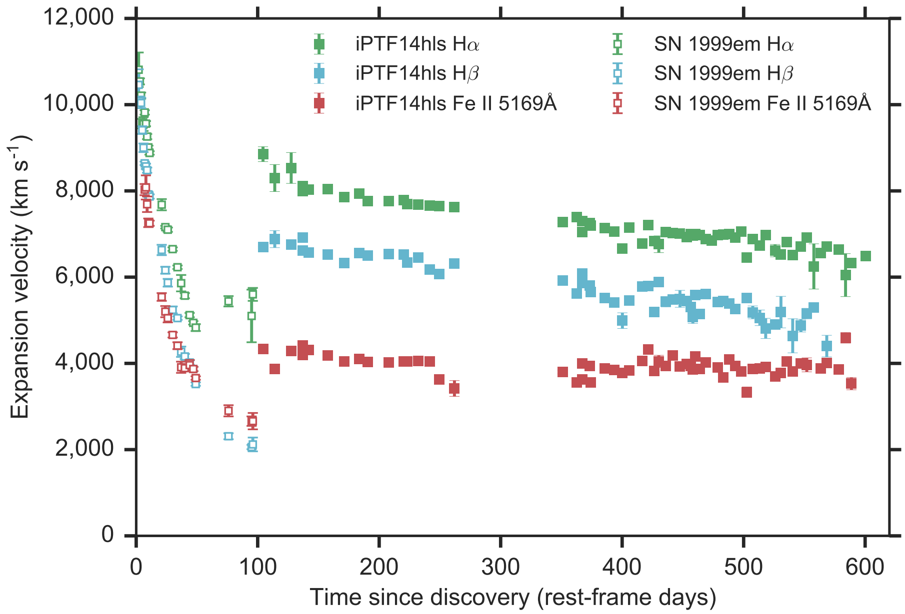

Figure 3 Expansion velocities as a function of time, measured from the P-Cygni absorption features of three different spectral lines (see Methods) for iPTF14hls (filled symbols) and the prototypical Type II-P SN 1999em[22] (empty symbols). Error bars denote 1σ uncertainties and are sometimes smaller than the marker size. The velocities seen for iPTF14hls evolve much more slowly compared to SN 1999em.

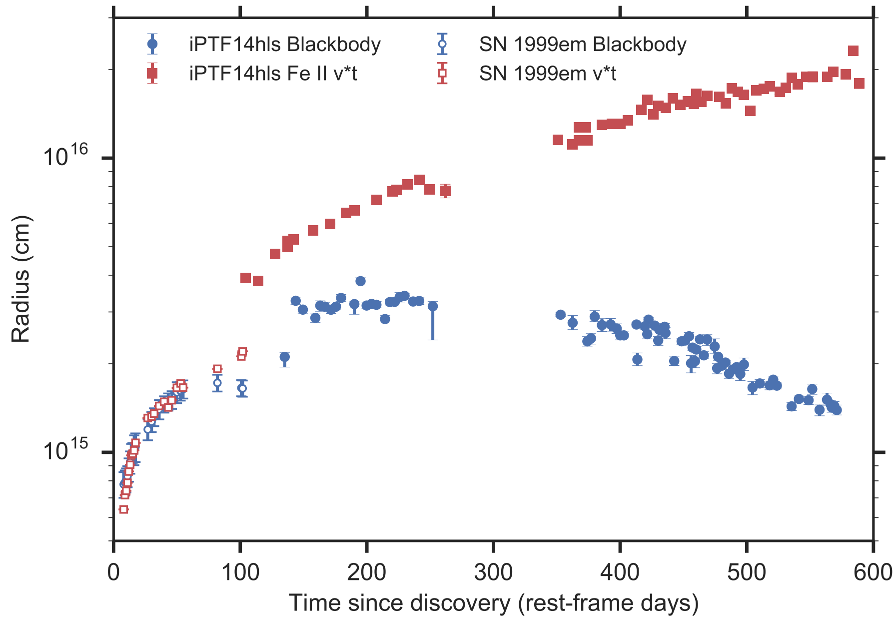

Figure 4 The photospheric radius of iPTF14hls (filled symbols) estimated in two different ways: (1) Using blackbody fits to the broad-band $BVgi$ photometry (blue) and (2) using the derived expansion velocities of Fe II 5169 Å (Fig. 3) times the elapsed rest-frame time since discovery (red). The same quantities are shown for the prototypical Type II-P SN 1999em (empty symbols; after correcting for the blackbody dilution factor)[22]. Error bars denote 1σ uncertainties and are sometimes smaller than the marker size. For SN 1999em the radii overlap as expected, but for iPTF14hls they diverge, indicating that the line-forming region may be detached from the photosphere (if the explosion occurred before discovery the divergence is even more extreme).

Supplementary Information

We are grateful to C. Harris, D. Leonard, D. Poznanski, N. Smith and S. Woosley for comments and discussion, and to T. Pursimo for assistance with the polarimetry measurements.

Support for I. Arcavi was provided by NASA through the Einstein Fellowship Program, grant PF6-170148. This research is funded in part by the Gordon and Betty Moore Foundation through Grant GBMF5076 to LB and DK and by the National Science Foundation under grant PHY 11-25915. DAH, GH, and CM are supported by NSF grant AST-1313484. AGY is supported by the EU via ERC grants No. 307260 and 725161, the Quantum Universe I-Core program by the Israeli Committee for Planning and Budgeting, and the ISF; a Binational Science Foundation ”Transformative Science” grant and by a Kimmel award. JS gratefully acknowledges support from the Knut and Alice Wallenberg Foundation. KM acknowledges funding from the Hintze Trust. XW, TZ, and JZ are supported by Major State Basic Research Development Program (2013CB834903), the National Natural Science Foundation of China (NSFC grants: 11325313, 11403096 and 11633002), and the Strategic Priority Research Program of Emergence of Cosmological Structures of the Chinese Academy of Sciences (grant No. XDB09000000). AVF's supernova group at U.C. Berkeley is supported by Gary & Cynthia Bengier, the Christopher R. Redlich Fund, the TABASGO Foundation, and NSF grant AST-1211916. Research support to I. Andreoni is provided by the Australian Astronomical Observatory (AAO). BS is supported by NASA through Hubble Fellowship grant HF-51348.001 awarded by the Space Telescope Science Institute, which is operated by the Association of Universities for Research in Astronomy, Inc., for NASA, under contract NAS 5-26555. TW-SH is supported by the DOE Computational Science Graduate Fellowship, grant number DEFG02-97ER25308. MS acknowledges support from EU/FP7-ERC grant 615929.

The Intermediate Palomar Transient Factory project is a scientific collaboration among the California Institute of Technology, Los Alamos National Laboratory, the University of Wisconsin, Milwaukee, the Oskar Klein Center, the Weizmann Institute of Science, the TANGO Program of the University System of Taiwan, and the Kavli Institute for the Physics and Mathematics of the Universe. LANL participation in iPTF was funded by the US Department of Energy as part of the Laboratory Directed Research and Development program. Part of this research was carried out at the Jet Propulsion Laboratory, California Institute of Technology, under a contract with the National Aeronautics and Space Administration. This paper made use of data from Las Cumbres Observatory global network of telescopes; the W. M. Keck Observatory, which is operated as a scientific partnership among the California Institute of Technology, the University of California, and NASA; the observatory was made possible by the generous financial support of the W. M. Keck Foundation; the Nordic Optical Telescope, operated by the Nordic Optical Telescope Scientific Association at the Observatorio del Roque de los Muchachos, La Palma, Spain, of the Instituto de Astrofisica de Canarias; ALFOSC, which is provided by the Instituto de Astrofisica de Andalucia (IAA) under a joint agreement with the University of Copenhagen and NOTSA; DOLoRes on TNG; the Discovery Channel Telescope (DCT) at Lowell Observatory. Lowell is a private, nonprofit institution dedicated to astrophysical research and public appreciation of astronomy and operates the DCT in partnership with Boston University, the University of Maryland, the University of Toledo, Northern Arizona University and Yale University. The upgrade of the DeVeny optical spectrograph has been funded by a generous grant from John and Ginger Giovale. We thank the support of the staffs at *Swift*, AMI-LA and the Xinglong Observatory (part of the National Astronomical Observatories of China) and the Lijiang Observatory (part of the Yunnan Observatories of China) for assistance with the observations. The AMI is supported by the European Research Council. Development of ASAS-SN has been supported by NSF grant AST-0908816 and CCAPP at the Ohio State University. ASAS-SN is supported by NSF grant AST-1515927, the Center for Cosmology and AstroParticle Physics (CCAPP) at OSU, the Mt. Cuba Astronomical Foundation, George Skestos, and the Robert Martin Ayers Sciences Fund. ASAS-SN thanks LCO and its staff for their continued support. The Digitized Sky Surveys were produced at the Space Telescope Science Institute under U.S. Government grant NAG W-2166. The National Geographic Society - Palomar Observatory Sky Atlas (POSS-I) was made by the California Institute of Technology with grants from the National Geographic Society. The Second Palomar Observatory Sky Survey (POSS-II) was made by the California Institute of Technology with funds from the National Science Foundation, the National Geographic Society, the Sloan Foundation, the Samuel Oschin Foundation, and the Eastman Kodak Corporation.

Methods

Discovery The intermediate Palomar Transient Factory (iPTF) first detected iPTF14hls on 2014 Sep 22.53 (Extended Data Fig. 1) using the iPTF real-time image-subtraction pipeline[23]. No source was seen at that position when it was previously visited by iPTF and by the All Sky Automated Survey for Supernova (ASAS-SN)[24] on 2014 May 6.19 and 2014 May 20-28 down to 3σ limiting magnitudes of $R < 20.95$ and $V < 18.7$, respectively. The source was observed by iPTF again on 2014 Oct. 13, Oct. 31, Nov. 4, and Nov. 10 before being saved and given a name as part of routine iPTF transient scanning. On 2014 Nov. 18, iPTF14hls was independently discovered by the Catalina Real-Time Transient Survey[25] as CSS141118:092034+504148, and later the event was reported to the Transient Name Server as AT 2016bse and Gaia16aog. On 2015 Feb. 3, upon routine LCO rescanning of previously saved iPTF candidates, we noticed the peculiar decline and subsequent rise of the light curve, and began an extensive campaign of spectroscopic and multi-band photometric follow-up observations.

Followup Imaging Followup imaging was obtained with the Palomar 48-inch Oschin Schmidt telescope (P48), the Palomar 60-inch telescope (P60)[26] using both the GRBCam and the SED Machine (SEDM) instruments, the Las Cumbres Observatory (LCO)[27] network 1-m and 2-m telescopes, and the 0.8-m Tsinghua University-NAOC telescope (TNT)[28] at the Xinglong Observatory. The TNT photometry is presented (together with CSS and Gaia photometry downloaded from their respective websites) in Extended Data Figure 2. P48 images were first pre-processed by the Infrared Processing and Analysis Center (IPAC)[29]. Image subtraction and point-spread-function (PSF) fitting was then performed[30] using pre-explosion images as templates. Magnitudes were calibrated to observations of the same field by the Sloan Digital Sky Survey (SDSS) DR10[31]. P60 images were pre-processed using a PyRAF-based pipeline[26]. Image subtraction, photometry extraction and calibration were performed with the `FPipe` pipeline[32] using SDSS images as references. LCO images were pre-processed using the Observatory Reduction and Acquisition Control Data Reduction pipeline (ORAC-DR)[33] up to 2016 May 4, and using the custom Python-based `BANZAI` pipeline afterward. Photometry was then extracted using the PyRAF-based `LCOsupernovapipe` pipeline[34] to perform PSF fitting and calibration to the AAVSO Photometric All-Sky Survey[35] for BV-band data and SDSS DR8[36] for gri-band data. TNT images were reduced with standard IRAF routines; PSF fitting was performed using the `SNOoPy` package and calibrated to the SDSS DR9[37] transformed to the Johnson system[38]. We correct all photometry for Milky Way extinction[39] extracted via the NASA Extragalactic Database (NED). Pre-explosion nondetection limits are presented in Extended Data Figure 3.

We fit a blackbody spectral energy distribution (SED) to every epoch of LCO photometry containing at least three of the *BVgi* filters obtained within 0.4 days of each other (we exclude r and R-band data from the fits owing to contamination from the Hα line). For each epoch we perform a blackbody fit using Markov Chain Monte Carlo simulations through the Python `emcee` package[40] to estimate the blackbody temperature and radius at the measured distance to iPTF14hls of 156 Mpc.

Followup Spectroscopy Spectra of iPTF14hls were obtained with the Floyds instrument mounted on the northern LCO 2-m telescope[27], the Andalucia Faint Object Spectrograph and Camera (ALFOSC) mounted on the 2.5-m Nordic Optical Telescope (NOT), the Device Optimized for the LOw

RESolution (DOLoRes) mounted on the 3.6-m Telescopio Nazionale Galileo (TNG), the Low Resolution Imaging Spectrometer (LRIS)[41] mounted on the Keck I 10-m telescope, the DEep Imaging Multi-Object Spectrograph (DEIMOS)[42] mounted on the Keck II 10-m telescope, the Double Beam Spectrograph (DBSP)[43] mounted on the Palomar 200-inch telescope (P200), the Beijing Faint Object Spectrograph and Camera (BFOSC) on the Xinglong 2.16-m telescope of the National Astronomical Observatories of China, the Yunnan Faint Object Spectrograph and Camera (YFOSC) on the Lijiang 2.4-m telescope of the Yunnan Observatories, and the DeVeny spectrograph mounted on the 4.3-m Discovery Channel Telescope (DCT). The Floyds spectra were reduced using the PyRAF-based `floydsspec` pipeline. The ALFOSC and DOLORES spectra were reduced using custom MATLAB pipelines. The LRIS spectra were reduced using the IDL `LPipe` pipeline. The DEIMOS spectrum was reduced using a modified version of the `DEEP2` pipeline[44,45] combined with standard PyRAF and IDL routines for trace extraction, flux calibration and telluric correction. The DBSP spectrum was reduced using custom IRAF and IDL routines. The BFOSC, YFOSC and DeVeny spectra were reduced using standard IRAF procedures. All spectra are available for download via WISeREP[46]. No Na I D absorption is seen at the redshift of the host galaxy, indicating very low host-galaxy extinction at the supernova position.

We fit each iPTF14hls spectrum to a library of Type II supernovae (which includes a full set of SN 1999em spectra[22]) using Superfit[47]. We then calculate the average best-fit supernova phase, weighing all the possible fits by their corresponding fit scores. We repeat this process for cutouts of the iPTF14hls spectra centered around the Hα, Hβ, and Fe II 5169Å features (separately). The weighted-average best-fit phases for each cutout are presented in Extended Data Figure 4.

iPTF14hls can be seen to evolve more slowly than other Type II supernovae by a factor of $\approx$10 when considering the entire spectrum, as well as when considering the Hβ and the Fe II 5169Å features separately, and by a factor of 6–7 when considering the Hα emission feature separately.

Expansion velocities for different elements in iPTF14hls were measured by fitting a parabola around the minimum of the absorption feature of their respective P-Cygni profiles. The difference between the minimum of the best-fit parabola and the rest wavelength of the line was translated to an expansion velocity. The endpoints of each parabolic fit were chosen manually for each line, so that they would remain the same for all spectra. Uncertainties in the velocities were estimated by randomly varying these endpoints by ± 5 Å around their original values.

Is iPTF14hls Powered by Interaction? As mentioned in the main text, interaction between supernova ejecta and a pre-existing dense CSM could cause an increase in luminosity. However, iPTF14hls does not display the spectral line profiles typically seen in such cases (Extended Data Figure 5).

In some interaction models the collision of the supernova ejecta and the CSM occurs outside the broad-line forming region, diluting the line emission. Focusing on the $\approx 50\%$ luminosity increase of iPTF14hls between rest-frame day 207 and 232 after discovery (Fig. 1), we find that the spectra taken on day 207 and day 232 are identical up to a global normalization factor. This indicates that the increase in luminosity is equal at all wavelengths, in contrast to the expected line dilution from interaction (Extended Data Figure 6).

Additional possible indicators of interaction are strong X-ray and/or radio emission. We observed the location of iPTF14hls with the X-Ray Telescope (XRT)[48] onboard the *Swift* satellite[49] on 2015 May 23.05. A total $4.9\,\mathrm{ks}$ of live exposure time was obtained on the source. We use on-line analysis tools[50, 51] to search for X-ray emission at the location of iPTF14hls. No source is detected with an upper limit on the 0.3–10.0 keV count rate of $< 2.3 \times 10^{-3}\,\mathrm{ct\,s^{-1}}$. Assuming a power-law spectrum with a photon index of $\Gamma = 2$ and a Galactic H column density[52] of $1.4 \times 10^{20}\,\mathrm{cm^{-2}}$, this corresponds to an upper limit on the unabsorbed 0.3–10.0 keV flux of $f_X < 8.4 \times 10^{-14}\,\mathrm{erg\,cm^{-2}\,s^{-1}}$. At the luminosity distance of iPTF14hls this corresponds to a luminosity limit of $L_X < 2.5 \times 10^{41}\,\mathrm{erg\,s^{-1}}$ (which is roughly 10^{-2} of the peak bolometric luminosity). The lack of X-ray emission disfavors strong interaction in iPTF14hls though some interacting supernovae display X-ray emission fainter than the limit we deduce here[53]. We observed iPTF14hls also with the Arcminute Microkelvin Imager Large Array (AMI-LA)[54] at 15 GHz on 2015 May 18.59, May 19.77, May 23.63, May 25.65, May 28.66, and May 31.62. 3C48 and J2035+1056 were used as the flux/bandpass and phase calibrators, respectively. RFI excision and calibration of the raw data was done with a fully automated pipeline `AMI-REDUCE`[55, 56]. The calibrated data for the supernova were imported into CASA and imaged independently for each epoch into 512×512 pixel maps ($4''$ per pixel) using the `clean` task. A similar imaging scheme was used for the concatenated data from all the epochs as well. The supernova was not detected on any of the individual epochs, with 3σ upper limits between 60–120 μJy. The combined 3σ upper limit is 36 μJy. There is a 5–10% absolute flux calibration uncertainty that we have not considered in these upper limits. On 2016 Jun 10, iPTF14hls was observed with the VLA at $6.1\,\mathrm{GHz}$. The

VLA data were reduced using standard CASA software routines where J0920+4441 and 3C286 were used as phase and flux calibrators. No radio emission was observed at the supernova position to a 3σ upper limit of $21.3\,\mu$Jy. At the luminosity distance of iPTF14hls, this corresponds to $6.2 \times 10^{26}\,\mathrm{erg\,s^{-1}\,Hz^{-1}}$, which is fainter than the radio emission of most interacting supernovae[53].

We conclude that iPTF14hls does not show any of the signatures seen in supernovae powered by interaction.

Is iPTF14hls Powered by a Central Engine? A central engine such as the spindown of a magnetar[57, 12, 58] or fallback accretion onto a black hole[59, 13] created after core collapse (assuming the material falling back has sufficient angular momentum to form a disk) could inject power to the supernova, although, as noted in the main text, this may fail to reproduce the observed iron and hydrogen line velocity difference. A magnetar (with an initial spin period of $\approx$5–10 ms and a magnetic field of $\approx(0.5\text{–}1)\times10^{14}$ Gauss) can produce the observed average luminosity and timescale of iPTF14hls[12]. However, the analytical magnetar light curve required to fit the late-time decline overpredicts the early-time emission of iPTF14hls (Extended Data Fig. 2) and produces a smooth rather than variable light curve[12, 13]. For a black hole central engine, on the other hand, instabilities in the accretion flow might produce strong light-curve variability, as seen in active galactic nuclei[20]. In this case, the light curve is expected to eventually settle onto a $t^{-5/3}$ decline rate[21] after the last instability. Such a decline rate is indeed observed for iPTF14hls starting on day ≈ 450 (Extended Data Fig. 2), supporting a black hole power source.

We conclude that iPTF14hls does not show the expected signatures of magnetar power (using available analytical models), but might be consistent with black hole accretion power.

Is iPTF14hls Assymetric? A possible explanation for the high luminosities and apparent emitted energy of iPTF14hls, as well as the discrepancy between its line-forming vs. blackbody radii, is strong assymetry in the explosion. Such assymetry would be indicated by a polarization signal.

We observed iPTF14hls with the Andalucia Faint Object Spectrograph and Camera (ALFOSC) mounted on the 2.5-m Nordic Optical Telescope (NOT) in polarimetric mode on 2015 Nov 03 in R-band, and Dec 15 in V-band (we also obtained observations on 2015 Oct 28 and Nov 14 but we discard them due to very poor observing conditions). We used a 1/2 wave plate in the FAPOL unit and a calcite plate mounted in the aperture wheel, and observed in 4 different retarder angles (0, 22.5, 45, 67.5 degrees). The data were reduced in a standard manner, using bias frames and flat-fields without the polarisation units in the light path. The field of view contains one bright star that can be used for calibration and for determining the interstellar polarisation (ISP) in the Galaxy. The low Galactic extinction towards iPTF14hls implies an expected ISP value of $< 0.13\%$[60]. To measure the fluxes we performed aperture photometry, and to compute the polarisation we followed standard procedures[61]. For our epoch with the best signal to noise (2015 Nov 03), we measure $P = 0.40 \pm 0.27\%$ for iPTF14hls and $P = 0.17 \pm 0.09\%$ for the comparison star, in agreement with the ISP prediction. These results suggest that iPTF14hls is close to spherically symmetric, similar to what is observed for Type II-P supernovae during their plateau phase[62]. The 2015 Dec 15 epoch yields a lower precision ($P = 1.1 \pm 0.7\%$ for iPTF14hls and $P = 0.80 \pm 0.23\%$ for the comparison star), but is still consistent with very low asphericity.

Why are the Expansion Velocities of iPTF14hls so Perplexing? In a supernova, the ejecta are in homologous expansion — that is, the radius of the ejecta at time t evolves as $r = vt$, with faster material at larger radii. Even for perfectly mixed ejecta, at any given time, spectral lines of different elements form in different regions. Specifically, the Fe lines are formed at smaller radii than the H lines and therefore display a lower velocity. This is also the case in iPTF14hls. As time passes and the ejecta expand and recombine, the line-forming region of each element moves inward in mass to a region where the outflow is slower. This is why, normally, the velocity of all lines is observed to decrease with time. Thus, following the line velocity over a wide range of time (and hence mass coordinates) provides a "scan" of the velocity profile over a large range of the ejecta. Although different lines are formed at different regions, all line-forming regions scan the velocity profile of the same ejecta. Therefore if there is a significant velocity gradient in the ejecta, we expect to see both a significant velocity difference between the Fe and H lines as well as significant evolution in the velocity of each line as the material expands. These two features are seen clearly in the typical case of SN 1999em (Extended Data Fig. 7). However, this is not the case in iPTF14hls. On the one hand there is a significant difference between the H and Fe line velocities, indicating a large velocity gradient in the ejecta. On the other hand, the velocity of each line shows almost no evolution in time between days 100 and 600 after discovery. If the line-forming material were ejected at discovery then this time span corresponds to a change by a factor of ≈ 6 in radius. In this case, the lack of observed velocity evolution indicates a very shallow velocity gradient in the ejecta, which is inconsistent with the large velocity difference between the lines. However, if the ejection of the line-forming material took place before discovery, then the relative change in radius during the observations is small, indicating that the position of the line-forming region does not change much, potentially solving the apparent contradiction.

The Line-Forming Region of iPTF14hls The nearly constant line velocities measured in iPTF14hls suggest that the lines form in a massive shell, perhaps ejected prior to the explosion. Here we estimate the mass and energetics required for such a shell to produce the observed line features.

Consider a uniform shell of mass M with a radius r and width Δr. The number density of hydrogen atoms in the shell is

$$n_{\rm H} = \frac{Y_H M}{\mu m_p 4\pi r^2 \Delta r} \tag{1}$$

where $Y_H \approx 0.9$ is the number fraction of hydrogen and $\mu \approx 1.34$ the mean atomic mass for solar gas (m_p is the proton mass). In a rapidly expanding, homologous outflow ejected at a time $t_{\rm ej}$, the strength of a spectral line is characterized by the Sobolev optical depth approximation

$$\tau_{\rm sob} = \frac{\pi e^2}{m_e c} n_l f t_{\rm ej} \lambda_0 \tag{2}$$

where n_l is the number density of atoms in the lower level, f is the line oscillation strength, $t_{\rm ej}$ is the time since explosion, and λ_0 is the line rest wavelength. For a line to produce a noticeable absorption component in the spectra, it must have $\tau_{\rm sob} \gtrsim 1$.

To estimate the populations in the lower level of the line transition (for the Balmer series this is the $n = 2$ level), we apply the nebular approximation[63], which assumes the mean intensity of the radiation field at a radius above a nearly blackbody photosphere is $J_\nu(r) = W(r) B_\nu(T_{\rm bb})$ where B_ν is the Planck function, $T_{\rm bb}$ is the temperature of the photosphere, and $W(r)$ is the geometrical dilution factor of the radiation field:

$$W(r) = \frac{1}{2}\left[1 - \sqrt{1 - r_p^2/r^2}\right] \approx \frac{r_p^2}{4r^2} \tag{3}$$

Here, r_p is the photospheric radius and the last expression assumes $r \gg r_p$. For a two-level atom subject to this radiation field, the number density in the $n = 2$ excited state is

$$n_2 \approx n_1 W \frac{g_2}{g_1} e^{-\Delta E_{1,2}/kT} \tag{4}$$

where n_1,n_2, and g_1,g_2 are (respectively) the number density and statistical weights of the $n = 1$ and $n = 2$ levels, and $\Delta E_{1,2}$ is the energy difference between the levels.

Since essentially all of the hydrogen in the shell will be neutral and in the ground state, $n_1 \approx n_{\mathrm{H}}$. The Sobolev optical depth is then

$$\tau_{H\alpha} \approx \left[\frac{\pi e^2}{m_e c} f \lambda_0 t_{\mathrm{ej}}\right] \frac{Y_H M}{\mu m_p} \frac{r_p^2}{16\pi r^4 \Delta r} \frac{g_2}{g_1} e^{-\Delta E_{1,2}/kT} \tag{5}$$

Using $g_1 = 2$, $g_2 = 8$, $\Delta E_{1,2} = 10.2\, eV$, $\lambda_0 = 6563\,\text{Å}$ (for the Hα transition), and $f = 0.64$, and taking $T = 6500\,\mathrm{K}$, $\Delta r = \Delta v t_{\mathrm{ej}}$ and $r = v t_{\mathrm{ej}}$ gives

$$\tau_{H\alpha} \approx 0.96 \left[\frac{M}{45\,\mathrm{M}_\odot}\right] \left[\frac{600\,\mathrm{days}}{t_{\mathrm{ej}}}\right]^4 \left[\frac{r_p}{1.5 \times 10^{15}\,\mathrm{cm}}\right]^2 \left[\frac{6000\,\mathrm{km\,s^{-1}}}{v}\right]^4 \left[\frac{1000\,\mathrm{km\,s^{-1}}}{\Delta v}\right] \tag{6}$$

Though approximate, this argument demonstrates that a shell with a mass of order a few tens of solar masses is likely required for producing Balmer absorption lines throughout the $\approx$ 600-day duration of the iPTF14hls light curve. The corresponding kinetic energy of the outburst is $\sim 10^{52}$ erg. In the case that the shell was ejected before the first iPTF14hls observations, the mass and energy required would increase. However, the mass required to associate the line forming region with the 1954 eruption would be $\sim 10^7\,\mathrm{M}_\odot$, and hence not reasonable, implying that the line forming region was ejected in a separate, more recent, eruption.

For comparison, the electron-scattering optical depth of the shell is

$$\tau_{\rm es} = n_{\rm H} x_{\rm HII} \sigma_T \Delta r \approx 0.77 x_{\rm HII} \left[\frac{M}{45\,\mathrm{M}_\odot}\right] \left[\frac{600\,\mathrm{days}}{t_{\rm ej}}\right]^2 \left[\frac{6000\,\mathrm{km\,s^{-1}}}{v}\right]^4 \tag{7}$$

where σ_T is the Thomson cross-section and $x_{\rm HII}$ is the fraction of ionized hydrogen. The shell will be largely neutral ($x_{\rm HII} \ll 1$), because the region where the radiation field is sufficient to ionize hydrogen occurs at the photosphere, r_p, where the recombination front forms. The shell radius is much larger than r_p, and so the radiation field is strongly diluted. Thus, while the shell can form line features, it will be optically thin in the continuum and allow most of the pseudo-blackbody continuum from the photosphere to pass through.

The velocity of $6000\,\mathrm{km\,s^{-1}}$ seen for Hα at day 600 after discovery, is seen for Hβ at day 200 after discovery. If we calculate the optical depth (Eq. 5) for Hβ, plugging in the parameters for day $200 + t_0$, and equate it to that of Hα at day $600 + t_0$ (where t_0 is the offset between the ejection of the shell and discovery), then we can solve for the ejection time t_0, assuming the optical depth for Hα and Hβ were the same when each was observed at $6000\,\mathrm{km\,s^{-1}}$, and that the entire shell was ejected simultaneously. Using $\lambda_0 = 4861\,\text{Å}$ and $f = 0.12$ for the Hβ transition, we find $t_0 \approx$100–200 days (the main source of error is the uncertainty in the precise temperature difference between the two epochs), meaning that the line-forming shell was ejected 100–200 days before discovery. We have deep non-detection limits for part of this epoch (Extended Data Fig. 3) suggesting that that the ejection of the shell could have been a low-luminosity event. This estimation of the ejection time, however, relies on many simplifying assumptions, so should be considered only as an approximation.

An Historical Outburst at the Position of iPTF14hls The Palomar Observatory Sky Survey (POSS)[64] observed the field of iPTF14hls on 1954 Feb. 23 in the blue and red filters. POSS-II[65] then re-observed the field on 1993 Jan. 2 in the blue filter and on 1995 Mar. 30 in the red filter. We obtained these images through the STScI Digitized Sky Survey and we find a source at the position of iPTF14hls in the blue image from POSS that is not present in the blue image from POSS-II (Extended Data Fig. 8). We do not see this source in either of the red images, but they are not as deep as the blue images (the limiting magnitude is roughly 20 for the red images compared to 21.1 for the blue images)[64].

We register the POSS blue image to the POSS-II blue image using the IRAF task `wregister`. We then use the `apphot` package in PyRAF, with a 3-pixel aperture, to measure the flux in six stars in the field near the position of iPTF14hls to determine a zero-point offset for the two images. We find an offset of 0.132 ± 0.050 mag. We then perform the same measurement around the nucleus of the host galaxy of iPTF14hls and find an offset of 0.141 mag, consistent with the zero-point offset. Next we perform the same aperture photometry measurement at the position of iPTF14hls in both images. We find a magnitude difference of 0.31 ± 0.14 over the host-galaxy level confirming the presence of an outburst in the 1954 image at the position of iPTF14hls at a 2.2σ confidence level. Owing to the nonlinear nature of the photographic plates used in the two POSS surveys, as well as differences between the filters[65], we cannot perform meaningful image subtraction between the POSS epochs to obtain more accurate photometric measurements. We consider this confidence level to be a conservative estimate, the outburst can be seen clearly by eye in the images (Extended Data Fig. 8).

We calibrate the six stars used for the zero-point comparison to SDSS u plus g-band fluxes (the POSS blue filter roughly covers the SDSS u and g bands)[64] and find that the magnitude of the 1954 outburst (after removing host-galaxy contribution) is $20.4 \pm 0.1\,(\mathrm{stat}) \pm 0.8\,(\mathrm{sys})$. The first error is statistical and due to photometric measurement uncertainties, while the second error is systematic and caused by the calibration to SDSS (the large error value is likely due to filter and detector differences between POSS and SDSS).

This corresponds to an absolute magnitude for the outburst of ≈ -15.6 at the luminosity distance of iPTF14hls (this is only a lower limit on the peak luminosity of the eruption, as we have only one epoch of observations). Such an eruption may be produced by the pulsational pair instability[2, 3, 4, 5]. Similar luminosity eruptions (though likely due to different instabilities) are inferred to be common in Type IIn supernova progenitors in the last year prior to explosion[66]. Spectra and broad-band colors are available for three such possible outbursts - a precursor to PTF10bjb[66], PTF13efv (a precursor to SNHunt275)[67] and the first 2012 outburst of SN 2009ip[68] - all of which display rather flat continuum emission, consistent with the limited color information we have for the 1954 outburst of iPTF14hls (i.e. the red non-detection limit being roughly 0.4 magnitudes brighter than the blue detection).

Given the host galaxy size of $\sim$10–100 times the centroiding error of the outburst, and a typical supernova rate of $\sim$100 per galaxy per year, there is a few percent probability that the detected outburst is an unrelated supernova that happened to occur at the position of iPTF14hls.

The Rate of iPTF14hls-like Events On 2014 Nov. 18, iPTF14hls was independently discovered by the Catalina Real-Time Transient Survey[25] as CSS141118:092034+504148, and more recently the event was reported to the Transient Name Server as AT 2016bse and Gaia16aog. The fact that it was discovered multiple times, but dismissed as a run of the mill SN II-P, is suggestive that similar events may have been missed in the past. We ourselves would not have noticed the unique properties of iPTF14hls had the iPTF survey scheduler not automatically continued to monitor the position of iPTF14hls. In addition, if iPTF14hls-like events are limited to low-mass galaxies, then targeted transient surveys would have missed them completely.

To our knowledge, iPTF14hls is the only supernova ever discovered to show such long-lived, slowly-evolving II-P-like emission. The PTF and iPTF surveys discovered 631 Type II supernovae, indicating that iPTF14hls-like events could be $\sim 10^{-3} - 10^{-2}$ of the Type II supernova rate. Since luminous long-lived varying events could be easier to detect in transient surveys compared to normal supernovae, the true volumetric rate of iPTF14hls-like events could be much lower. On the other hand, we cannot rule out whether such events were discovered in the past but dismissed as normal Type II-P supernovae after one spectrum with no subsequent followup or as possible AGN due to the light curve behavior. It is therefore not possible to calculate a precise rate for iPTF14hls-like events based on this single discovery, but whatever the explosion channel, it is likely to be rare. Even so, the Large Synoptic Survey Telescope could find hundreds of iPTF14hls-like events in its decade-long survey of the transient sky (more so if iPTF14hls-like events are more common in the early Universe, as is indicated by the possible low-metallicity environment of iPTF14hls).

The Host Galaxy of iPTF14hls We obtained a spectrum of the host galaxy of iPTF14hls on 2015 Dec 11 with the Low Resolution Imaging Spectrometer (LRIS)[41] mounted on the Keck I 10-m telescope. The spectrum was reduced using the standard techniques optimized for Keck+LRIS by the `CarPy` package in PyRAF, and flux calibrated to spectrophotometric standard stars obtained on the night of our observations in the same instrument configuration. The host galaxy spectrum, which is available for download via WISeREP[46], shows clear detections of Hα, Hβ, [O II] 3727Å and [O III] 4958,5007Å which we use to determine the redshift of 0.0344. A faint detection of [N II] 6583Å is also possible, but because the continuum is contaminated by broad Hα emission from the nearby supernova this feature is difficult to confirm. All of the lines are weak (equivalent width < 20Å) and no other lines are significantly detected. We extracted the fluxes of all lines by fitting Gaussians to their profiles (Extended Table 1), and calculated the metallicity by fitting[69] the line-strength ratios using several different diagnostics and calibrations (Extended Table 2). We find a range of metallicity estimates of $12 + \log$(O/H) $=$8.3–8.6, corresponding to ≈0.4–0.9 $\mathrm{Z}_{\odot}$ (where $\mathrm{Z}_{\odot}$ is the solar metallicity)[70]. A low metallicity could help explain how the progenitor of iPTF14hls retained a very massive hydrogen envelope. Future more direct environment studies will be able to better probe the metallicity at the explosion site.

We fit the SDSS $ugriz$ photometry of the host galaxy[71] with standard SED fitting techniques[72] using the BC03[73] stellar population synthesis models. Assuming a metallicity of $0.5\,\mathrm{Z}_{\odot}$, the best fit total stellar mass is $3.2 \pm 0.5 \times 10^{8}\,\mathrm{M}_{\odot}$, similar to that of the Small Magellanic Cloud.

23. Cao, Y., Nugent, P. E. & Kasliwal, M. M. Intermediate Palomar Transient Factory: Realtime Image Subtraction Pipeline. *eprint arXiv:1608.01006* (2016). URL http://arxiv.org/abs/1608.01006. 1608.01006.

24. Shappee, B. J. *et al.* the Man Behind the Curtain: X-Rays Drive the Uv Through Nir Variability in the 2013 Active Galactic Nucleus Outburst in Ngc 2617. *The Astrophysical Journal* **788**, 48 (2014). URL http://arxiv.org/abs/1310.2241http://dx.doi.org/10.1088/0004-637X/788/1/48http://adsabs.harvard.edu/abs/2014ApJ...788...48S. 1310.2241.

25. Drake, A. J. *et al.* First Results from the Catalina Real-time Transient Survey. *The Astrophysical Journal* **696**, 870–884 (2009). URL http://arxiv.org/abs/0809.1394http://dx.doi.org/10.1088/0004-637X/696/1/870. 0809.1394.

26. Cenko, S. B. *et al.* The Automated Palomar 60 Inch Telescope. *Publications of the Astronomical Society of the Pacific* **118**, 1396–1406 (2006). 0608323.

27. Brown, T. M. *et al.* Las Cumbres Observatory Global Telescope Network. *Publications of the Astronomical Society of Pacific, Volume 125, Issue 931, pp. 1031-1055 (2013).* **125**, 1031–1055 (2013). URL http://arxiv.org/abs/1305.2437http://dx.doi.org/10.1086/673168. 1305.2437.

28. Huang, F. *et al.* The photometric system of the Tsinghua-NAOC 80-cm telescope at NAOC Xinglong Observatory. *Research in Astronomy and Astrophysics, Volume 12, Issue 11, pp. 1585-1596 (2012).* **12**, 1585–1596 (2012). 1205.6529.

29. Laher, R. R. *et al.* IPAC Image Processing and Data Archiving for the Palomar Transient Factory. *Publications of the Astronomical Society of the Pacific* **126**, 674–710 (2014). 1404.1953.

30. Sullivan, M. *et al.* Photometric Selection of High-Redshift Type Ia Supernova Candidates. *The Astronomical Journal* **131**, 960–972 (2006). 0510857.

31. Ahn, C. P. *et al.* The Tenth Data Release of the Sloan Digital Sky Survey: First Spectroscopic Data from the SDSS-III Apache Point Observatory Galactic Evolution Experiment. *The Astrophysical Journal Supplement Series* **211** (2014). 1307.7735.

32. Fremling, C. *et al.* PTF12os and iPTF13bvn. Two stripped-envelope supernovae from low-mass progenitors in NGC 5806. *eprint arXiv:1606.03074* (2016). URL http://arxiv.org/abs/1606.03074. 1606.03074.

33. Jenness, T. & Economou, F. ORAC-DR: A generic data reduction pipeline infrastructure. *Astronomy and Computing* **9**, 40–48 (2015). 1410.7509.

34. Valenti, S. *et al.* The diversity of Type II supernova versus the similarity in their progenitors. *Monthly Notices of the Royal Astronomical Society, Volume 459, Issue 4, p.3939-3962* **459**, 3939–3962 (2016). URL http://arxiv.org/abs/1603.08953http://dx.doi.org/10.1093/mnras/stw870. 1603.08953.

35. Henden, A. A., Welch, D. L., Terrell, D. & Levine, S. E. The AAVSO Photometric All-Sky Survey (APASS) (2009).

36. Aihara, H. *et al.* The Eighth Data Release of the Sloan Digital Sky Survey: First Data from SDSS-III. *The Astrophysical Journal Supplement Series* **193** (2011). `1101.1559`.

37. Ahn, C. P. *et al.* The Ninth Data Release of the Sloan Digital Sky Survey: First Spectroscopic Data from the SDSS-III Baryon Oscillation Spectroscopic Survey. *The Astrophysical Journal Supplement, Volume 203, Issue 2, article id. 21, 13 pp. (2012).* **203** (2012). URL `http://arxiv.org/abs/1207.7137http://dx.doi.org/10.1088/0067-0049/203/2/21`. `1207.7137`.

38. Chonis, T. S. & Gaskell, C. M. Setting UBVRI Photometric Zero-Points Using Sloan Digital Sky Survey ugriz Magnitudes. *The Astronomical Journal, Volume 135, Issue 1, pp. 264-267 (2008).* **135**, 264–267 (2008). `0710.5801`.

39. Schlafly, E. F. & Finkbeiner, D. P. Measuring Reddening with SDSS Stellar Spectra and Recalibrating SFD. *The Astrophysical Journal, Volume 737, Issue 2, article id. 103, 13 pp. (2011).* **737** (2011). URL `http://arxiv.org/abs/1012.4804http://dx.doi.org/10.1088/0004-637X/737/2/103`. `1012.4804`.

40. Foreman-Mackey, D., Hogg, D. W., Lang, D. & Goodman, J. emcee: The MCMC Hammer. *Publications of the Astronomical Society of Pacific, Volume 125, Issue 925, pp. 306-312 (2013).* **125**, 306–312 (2012). URL `http://arxiv.org/abs/1202.3665http://dx.doi.org/10.1086/670067`. `1202.3665`.

41. Oke, J. B. *et al.* The Keck Low-Resolution Imaging Spectrometer. *Publications of the Astronomical Society of the Pacific* **107**, 375 (1995). URL `http://www.jstor.org/`

stable/10.2307/40680546.

42. Faber, S. M. *et al.* The DEIMOS spectrograph for the Keck II Telescope: integration and testing. In Iye, M. & Moorwood, A. F. M. (eds.) *Instrument Design and Performance for Optical/Infrared Ground-based Telescopes. Edited by Iye, Masanori; Moorwood, Alan F. M. Proceedings of the SPIE, Volume 4841, pp. 1657-1669 (2003).*, vol. 4841, 1657–1669 (2003). URL http://proceedings.spiedigitallibrary.org/proceeding.aspx?articleid=874397.

43. Oke, J. B. & Gunn, J. E. An Efficient Low Resolution and Moderate Resolution Spectrograph for the Hale Telescope. *Publications of the Astronomical Society of the Pacific* **94**, 586 (1982). URL http://www.jstor.org/stable/10.2307/40677999.

44. Cooper, M. C., Newman, J. A., Davis, M., Finkbeiner, D. P. & Gerke, B. F. spec2d: DEEP2 DEIMOS Spectral Pipeline. *Astrophysics Source Code Library, record ascl:1203.003* (2012).

45. Newman, J. A. *et al.* The DEEP2 Galaxy Redshift Survey: Design, Observations, Data Reduction, and Redshifts. *The Astrophysical Journal Supplement, Volume 208, Issue 1, article id. 5, 57 pp. (2013).* **208** (2012). URL http://arxiv.org/abs/1203.3192http://dx.doi.org/10.1088/0067-0049/208/1/5. 1203.3192.

46. Yaron, O. & Gal-Yam, A. WISeREP - An Interactive Supernova Data Repository. *Publications of the Astronomical Society of Pacific, Volume 124, Issue 917, pp. 668-681 (2012).* **124**, 668–681 (2012). URL http://arxiv.org/abs/1204.1891http://dx.doi.org/10.1086/666656. 1204.1891.

47. Howell, D. A. *et al.* Gemini Spectroscopy of Supernovae from SNLS: Improving High Redshift SN Selection and Classification. *The Astrophysical Journal, Volume 634, Issue 2, pp. 1190-1201.* **634**, 1190–1201 (2005). URL http://arxiv.org/abs/astro-ph/0509195http://dx.doi.org/10.1086/497119. 0509195.

48. Burrows, D. N. *et al.* The Swift X-ray Telescope. *Space Science Reviews* **120**, 165–195 (2005). URL http://arxiv.org/abs/astro-ph/0508071http://dx.doi.org/10.1007/s11214-005-5097-2. 0508071.

49. Gehrels, N. *et al.* The Swift GammaRay Burst Mission. *The Astrophysical Journal* **611**, 1005–1020 (2004). URL http://stacks.iop.org/0004-637X/611/i=2/a=1005.

50. Evans, P. A. *et al.* An online repository of Swift/XRT light curves of GRBs. *Astronomy and Astrophysics* **469**, 379–385 (2007). URL http://arxiv.org/abs/0704.0128http://dx.doi.org/10.1051/0004-6361:20077530. 0704.0128.

51. Evans, P. A. *et al.* Methods and results of an automatic analysis of a complete sample of Swift-XRT observations of GRBs. *Monthly Notices of the Royal Astronomical Society* **397**, 1177–1201 (2009). URL http://arxiv.org/abs/0812.3662http://dx.doi.org/10.1111/j.1365-2966.2009.14913.x. 0812.3662.

52. Willingale, R., Starling, R. L. C., Beardmore, A. P., Tanvir, N. R. & O'Brien, P. T. Calibration of X-ray absorption in our Galaxy. *Monthly Notices of the Royal Astronomical Society* **431**, 394–404 (2013). URL http://arxiv.org/abs/1303.0843http://dx.doi.org/10.1093/mnras/stt175. 1303.0843.

53. Margutti, R. *et al.* Ejection of the massive Hydrogen-rich envelope timed with the collapse of the stripped SN2014C. *eprint arXiv:1601.06806* (2016). URL http://arxiv.org/abs/1601.06806. 1601.06806.

54. Zwart, J. T. L. *et al.* The Arcminute Microkelvin Imager. *Monthly Notices of the Royal Astronomical Society, Volume 391, Issue 4, pp. 1545-1558.* **391**, 1545–1558 (2008). URL http://arxiv.org/abs/0807.2469http://dx.doi.org/10.1111/j.1365-2966.2008.13953.x. 0807.2469.

55. Davies, M. L. *et al.* Follow-up observations at 16 and 33 GHz of extragalactic sources from WMAP 3-year data: I - Spectral properties. *Monthly Notices of the Royal Astronomical Society, Volume 400, Issue 2, pp. 984-994.* **400**, 984–994 (2009). URL http://arxiv.org/abs/0907.3707http://dx.doi.org/10.1111/j.1365-2966.2009.15518.x. 0907.3707.

56. Perrott, Y. C. *et al.* AMI Galactic Plane Survey at 16 GHz: I – Observing, mapping and source extraction. *Monthly Notices of the Royal Astronomical Society, Volume 429, Issue 4, p.3330-3340* **429**, 3330–3340 (2013). URL http://arxiv.org/abs/1208.5343http://dx.doi.org/10.1093/mnras/sts589. 1208.5343.

57. Ostriker, J. P. & Gunn, J. E. On the Nature of Pulsars. I. Theory. *The Astrophysical Journal* **157**, 1395 (1969). URL http://adsabs.harvard.edu/doi/10.1086/150160.

58. Woosley, S. E. Bright Supernovae From Magnetar Birth. *The Astrophysical Journal* **719**, L204–L207 (2010). URL http://adsabs.harvard.edu/abs/2010ApJ...719L.

204W.

59. Colgate, S. A. Neutron-Star Formation, Thermonuclear Supernovae, and Heavy-Element Reimplosion. *The Astrophysical Journal* **163**, 221 (1971). URL http://adsabs.harvard.edu/doi/10.1086/150760.

60. Serkowski, K., Mathewson, D. L. & Ford, V. L. Wavelength dependence of interstellar polarization and ratio of total to selective extinction. *The Astrophysical Journal* **196**, 261 (1975). URL http://adsabs.harvard.edu/doi/10.1086/153410.

61. Patat, F. & Romaniello, M. Error Analysis for Dual-Beam Optical Linear Polarimetry. *The Publications of the Astronomical Society of the Pacific, Volume 118, Issue 839, pp. 146-161.* **118**, 146–161 (2006). URL http://arxiv.org/abs/astro-ph/0509153http://dx.doi.org/10.1086/497581. 0509153.

62. Leonard, D. C. & Filippenko, A. V. Spectropolarimetry of the Type II Supernovae 1997ds, 1998A, and 1999gi. *The Publications of the Astronomical Society of the Pacific, Volume 113, Issue 786, pp. 920-936.* **113**, 920–936 (2001). 0105295.

63. Abbott, D. C. & Lucy, L. B. Multiline transfer and the dynamics of stellar winds. *The Astrophysical Journal* **288**, 679 (1985). URL http://adsabs.harvard.edu/doi/10.1086/162834.

64. Minkowski, R. L. & Abell, G. O. The National Geographic Society-Palomar Observatory Sky Survey. *Basic Astronomical Data: Stars and stellar systems, edited by K. A. Strand. Published by the University of Chicago Press, Chicago, IL USA, 1968, p.481* 481 (1963).

65. Reid, I. N. *et al.* The second Palomar Sky Survey. *Publications of the Astronomical Society of the Pacific* **103**, 661 (1991). URL http://www.jstor.org/stable/10.2307/40651696.

66. Ofek, E. O. *et al.* Precursors prior to Type IIn supernova explosions are common: precursor rates, properties, and correlations. *The Astrophysical Journal, Volume 789, Issue 2, article id. 104, 15 pp. (2014).* **789** (2014). URL http://arxiv.org/abs/1401.5468http://dx.doi.org/10.1088/0004-637X/789/2/104. 1401.5468.

67. Ofek, E. O. *et al.* PTF13efvAn Outburst 500 Days Prior to the SNHunt 275 Eexplosion and its Radiative Efficiency. *The Astrophysical Journal* **824**, 6 (2016). URL http://stacks.iop.org/0004-637X/824/i=1/a=6?key=crossref.00771ff6ff8d40ebf094f40e98f1d67c.

68. Fraser, M. *et al.* SN 2009ip a la PESSTO: No Evidence for Core-Collapse Yet. *Monthly Notices of the Royal Astronomical Society, Volume 433, Issue 2, p.1312-1337* **433**, 1312–1337 (2013). URL http://arxiv.org/abs/1303.3453http://dx.doi.org/10.1093/mnras/stt813. 1303.3453.

69. Bianco, F. B. *et al.* Monte Carlo Method for Calculating Oxygen Abundances and Their Uncertainties from Strong-Line Flux Measurements. *Astronomy and Computing, Volume 16, p. 54-66.* **16**, 54–66 (2016). URL http://arxiv.org/abs/1505.06213. 1505.06213.

70. Asplund, M., Grevesse, N., Sauval, A. J. & Scott, P. The chemical composition of the Sun. *Annual Review of Astronomy & Astrophysics, vol. 47, Issue 1, pp.481-522* **47**, 481–522 (2009). URL `http://arxiv.org/abs/0909.0948http://dx.doi.org/10.1146/annurev.astro.46.060407.145222`. `0909.0948`.

71. Alam, S. *et al.* The Eleventh and Twelfth Data Releases of the Sloan Digital Sky Survey: Final Data from SDSS-III. *The Astrophysical Journal Supplement Series, Volume 219, Issue 1, article id. 12, 27 pp. (2015).* **219** (2015). URL `http://arxiv.org/abs/1501.00963http://dx.doi.org/10.1088/0067-0049/219/1/12`. `1501.00963`.

72. Perley, D. A. *et al.* A Population of Massive, Luminous Galaxies Hosting Heavily Dust-Obscured Gamma-Ray Bursts: Implications for the Use of GRBs as Tracers of Cosmic Star Formation. *The Astrophysical Journal, Volume 778, Issue 2, article id. 128, 35 pp. (2013).* **778** (2013). URL `http://arxiv.org/abs/1301.5903http://dx.doi.org/10.1088/0004-637X/778/2/128`. `1301.5903`.

73. Bruzual, G. & Charlot, S. Stellar population synthesis at the resolution of 2003. *Monthly Notices of the Royal Astronomical Society, Volume 344, Issue 4, pp. 1000-1028.* **344**, 1000–1028 (2003). URL `http://arxiv.org/abs/astro-ph/0309134http://dx.doi.org/10.1046/j.1365-8711.2003.06897.x`. `0309134`.

74. Nagao, T., Maiolino, R. & Marconi, A. Gas metallicity diagnostics in star-forming galaxies. *Astronomy and Astrophysics, Volume 459, Issue 1, November III 2006, pp.85-101*

459, 85–101 (2006). URL http://arxiv.org/abs/astro-ph/0603580http://dx.doi.org/10.1051/0004-6361:20065216. 0603580.

75. Denicolo, G., Terlevich, R. & Terlevich, E. New light on the search for low metallicity galaxies I. The N2 method. *Monthly Notices of the Royal Astronomical Society, Volume 330, Issue 1, pp. 69-74.* **330**, 69–74 (2002). URL http://arxiv.org/abs/astro-ph/0110356http://dx.doi.org/10.1046/j.1365-8711.2002.05041.x. 0110356.

76. Pettini, M. & Pagel, B. E. J. [O III]/[N II] as an Abundance Indicator at High Redshift. *Monthly Notices of the Royal Astronomical Society, Volume 348, Issue 3, pp. L59-L63.* **348**, L59–L63 (2004). URL http://arxiv.org/abs/astro-ph/0401128http://dx.doi.org/10.1111/j.1365-2966.2004.07591.x. 0401128.

77. Maiolino, R. *et al.* AMAZE. I. The evolution of the mass-metallicity relation at z>3. *Astronomy and Astrophysics, Volume 488, Issue 2, 2008, pp.463-479* **488**, 463–479 (2008). URL http://arxiv.org/abs/0806.2410http://dx.doi.org/10.1051/0004-6361:200809678. 0806.2410.

78. Marino, R. A. *et al.* The O3N2 and N2 abundance indicators revisited: improved calibrations based on CALIFA and Te-based literature data. *Astronomy & Astrophysics, Volume 559, id.A114, 12 pp.* **559** (2013). URL http://arxiv.org/abs/1307.5316http://dx.doi.org/10.1051/0004-6361/201321956. 1307.5316.

79. Kobulnicky, H. A. & Kewley, L. J. Metallicities of 0.3. *The Astrophysical Journal, Volume 617, Issue 1, pp. 240-261*. **617**, 240–261 (2004). URL http://arxiv.org/abs/astro-ph/0408128http://dx.doi.org/10.1086/425299. 0408128.

80. Kewley, L. J. & Dopita, M. A. Using Strong Lines to Estimate Abundances in Extragalactic HII Regions and Starburst Galaxies. *The Astrophysical Journal Supplement Series, Volume 142, Issue 1, pp. 35-52*. **142**, 35–52 (2002). URL http://arxiv.org/abs/astro-ph/0206495http://dx.doi.org/10.1086/341326. 0206495.

Extended Data

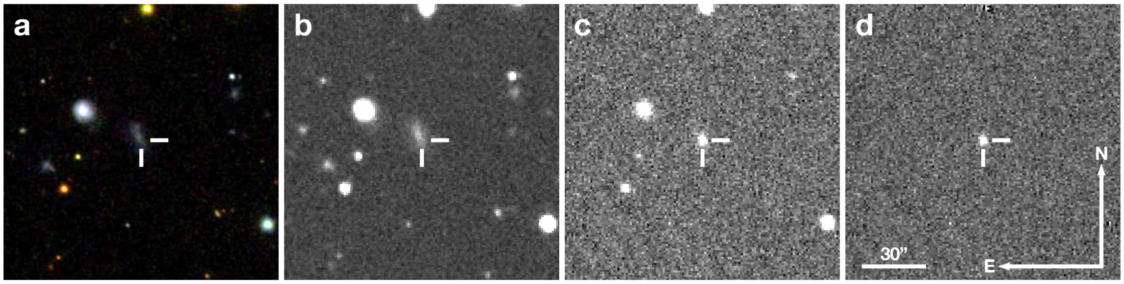

Extended Data Figure 1 The discovery and environment of iPTF14hls: (**a**) SDSS image centered at the position of iPTF14hls. (**b**) Palomar 48-inch deep coadded pre-discovery reference image. (**c**) Palomar 48-inch discovery image of iPTF14hls. (**d**) The result of subtracting the reference image from the discovery image. The position of iPTF14hls is indicated by tick marks in each image.

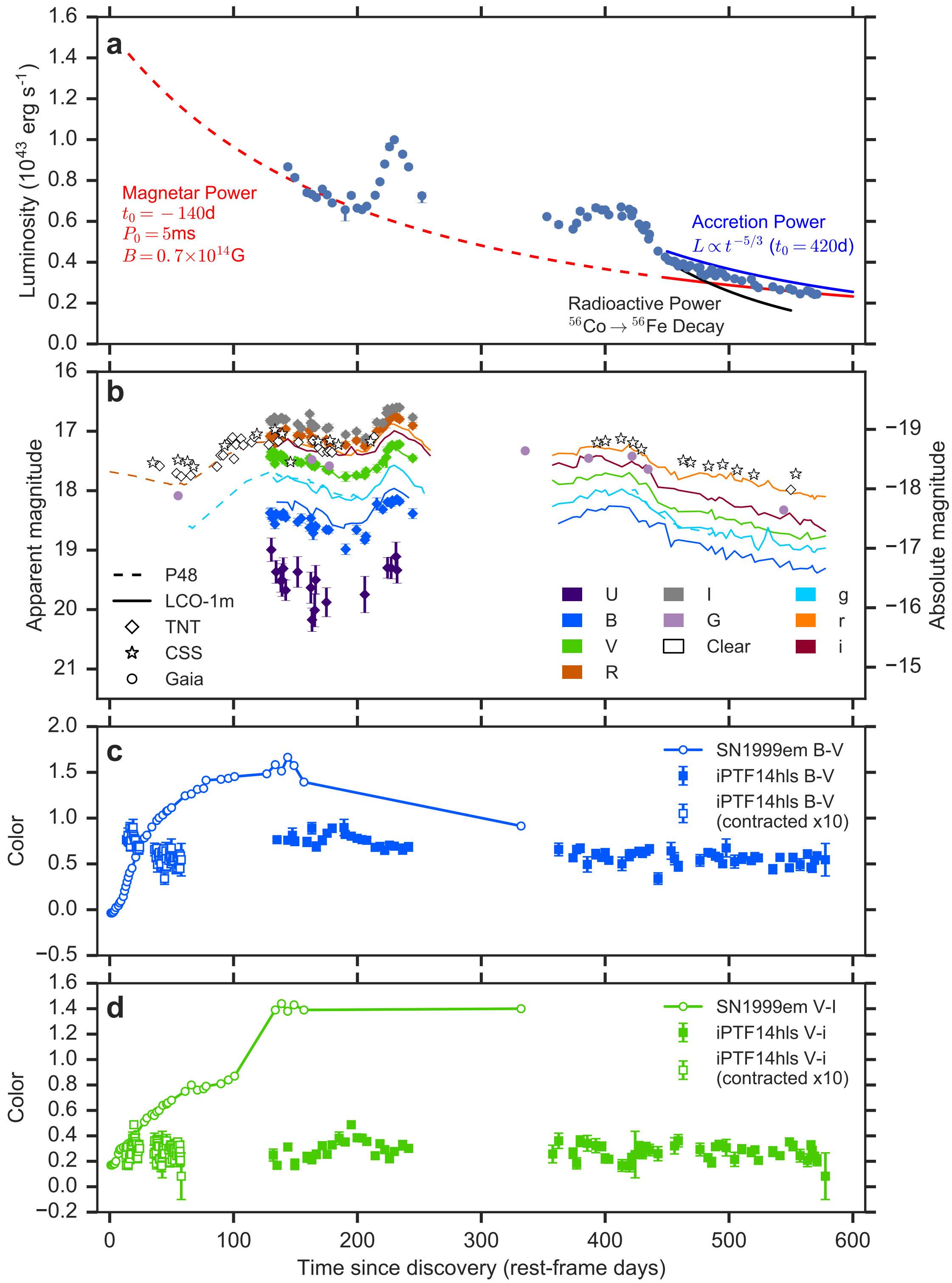

Extended Data Figure 2 The bolometric light curve of iPTF14hls (**a**) deduced from the blackbody fits shows a late-time decline rate which is slower than the radioactive decay of ^{56}Co (black), but consistent with both accretion power (blue; t_0 is the onset of accretion at the last peak) and magnetar spindown power (red; t_0 is the formation time of the magnetar, P_0 is the initial spin period and B is the magnetic field in this simple analytic model). The magnetar model, however, is not consistent with the luminosity during the first 100 days, as implied by the P48, CSS and Gaia observations (**b**), unless the early-time magnetar emission is significantly adiabatically degraded. TNT photometry of iPTF14hls and publicly available CSS and Gaia photometry (**b**), not presented in Figure 1. Data from the P48 (dashed lines) and the LCO 1-m telescope (solid lines) presented in Figure 1 are shown for comparison. Photometric points from the same day, instrument, and filter are averaged for clarity. Error bars, available only for the TNT data, denote 1σ uncertainties. The *B-V* (**c**) and *V-I/i* (**d**) color evolution of iPTF14hls from the LCO 1-m data (filled squares) differs from that of the normal Type II-P SN 1999em (empty circles)[22], even when contracting the iPTF14hls data by a factor of 10 in time (empty squares) to compensate for the slowed down evolution observed in its spectra compared to normal II-P supernovae.

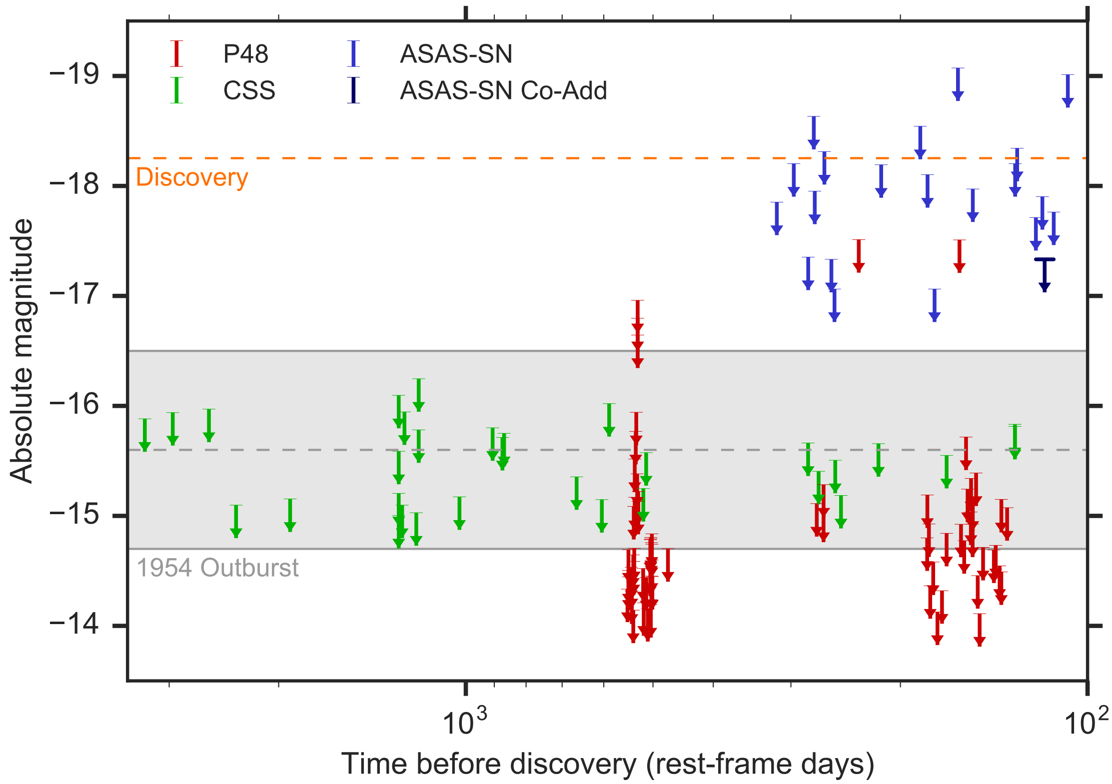

Extended Data Figure 3 Pre-explosion nondetection limits for iPTF14hls from P48 (R band, 3σ nondetections), CSS (unfiltered, obtained via the CSS website) and ASAS-SN (V-band, 3σ non-detections — the dark-blue arrow is a deep coadd of the three images taken during the time range denoted by the horizontal line in the marker). The dashed line denotes the discovery magnitude and the shaded region denotes the 1954 outburst magnitude and its uncertainty.

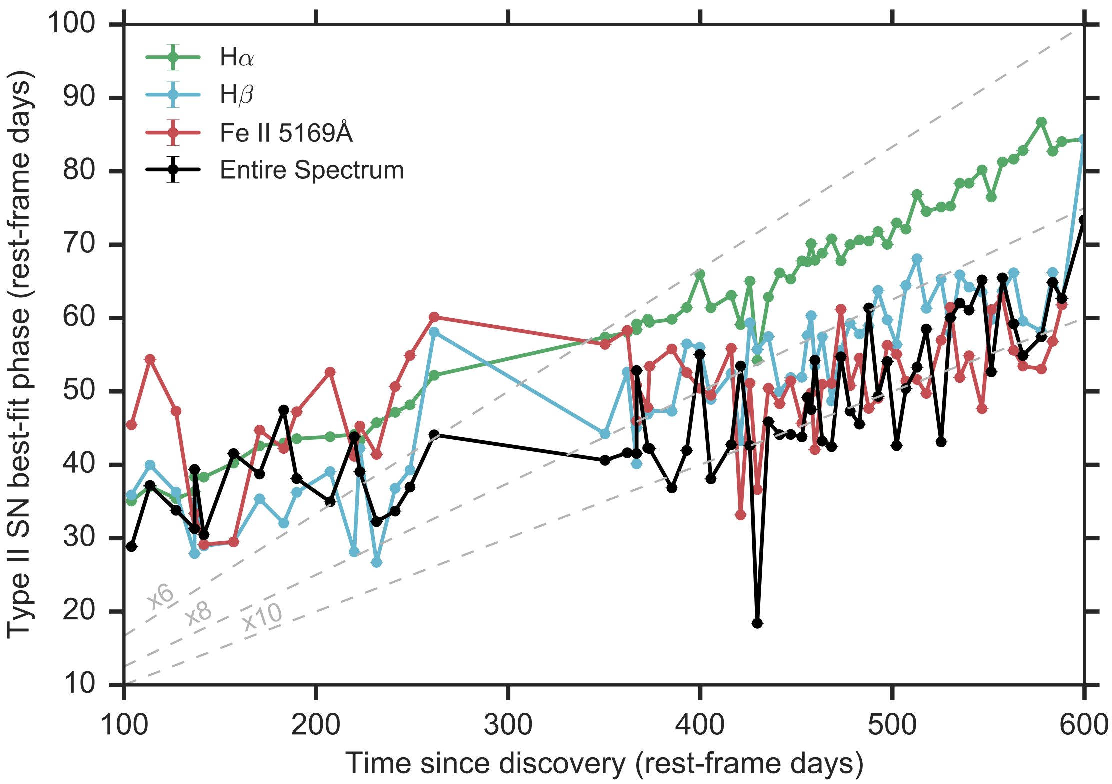

Extended Data Figure 4 Weighted average best-fit phase of iPTF14hls spectra from Superfit[47], compared to the true spectral phase, when fitting the entire spectrum (black) or only certain line regions as noted. The dashed lines denote constant ratios between the observed and best-fit phases (assuming the explosion happened at discovery). The spectra of iPTF14hls are a factor of ≈6–10 slower evolving compared to other Type II supernovae.

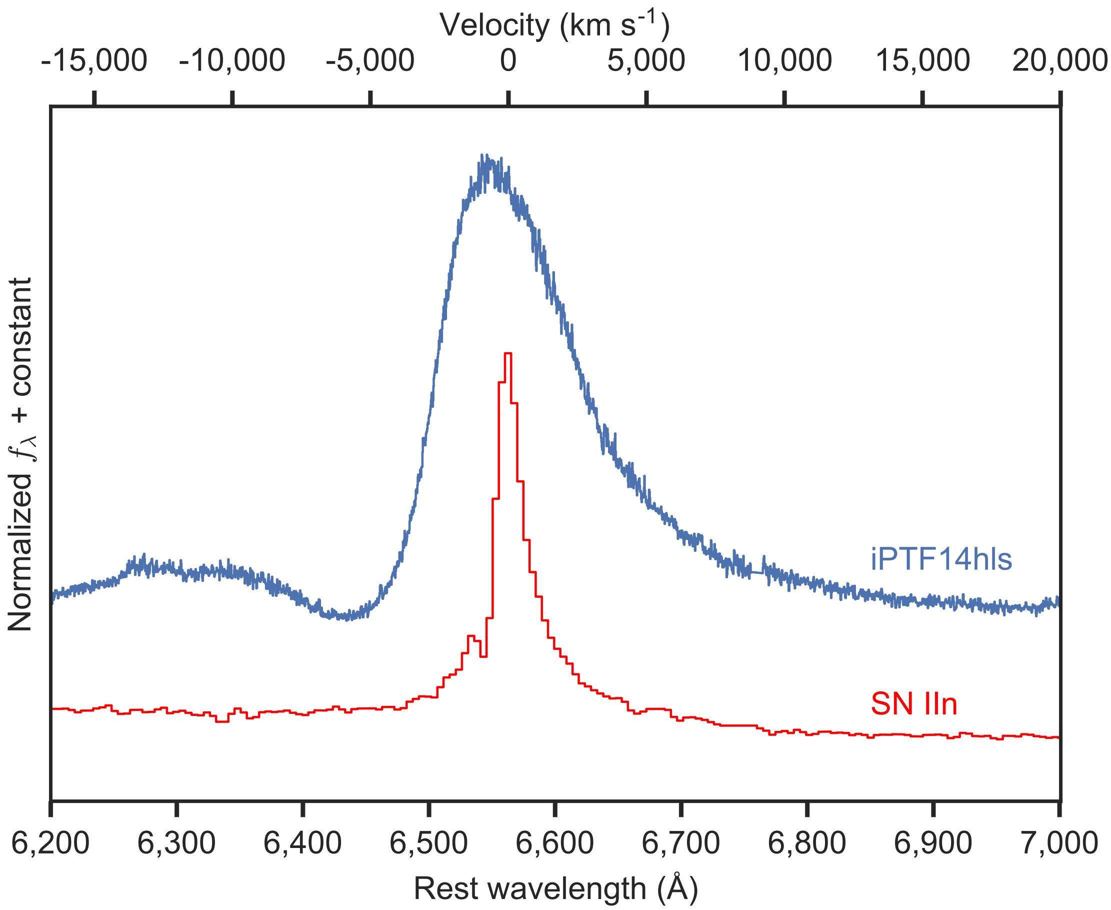

Extended Data Figure 5 The Hα region in our highest-resolution spectrum of iPTF14hls taken on 2016 June 4 using DEIMOS on Keck II (blue), expressed in terms of normalized flux density as a function of rest-frame wavelength (bottom axis), compared to the interaction-powered Type IIn supernova 2005cl[18] (red). The top axis is the corresponding velocity of Hα. iPTF14hls shows no signs of the narrow emission or narrow P-Cygni features seen in interacting supernovae.

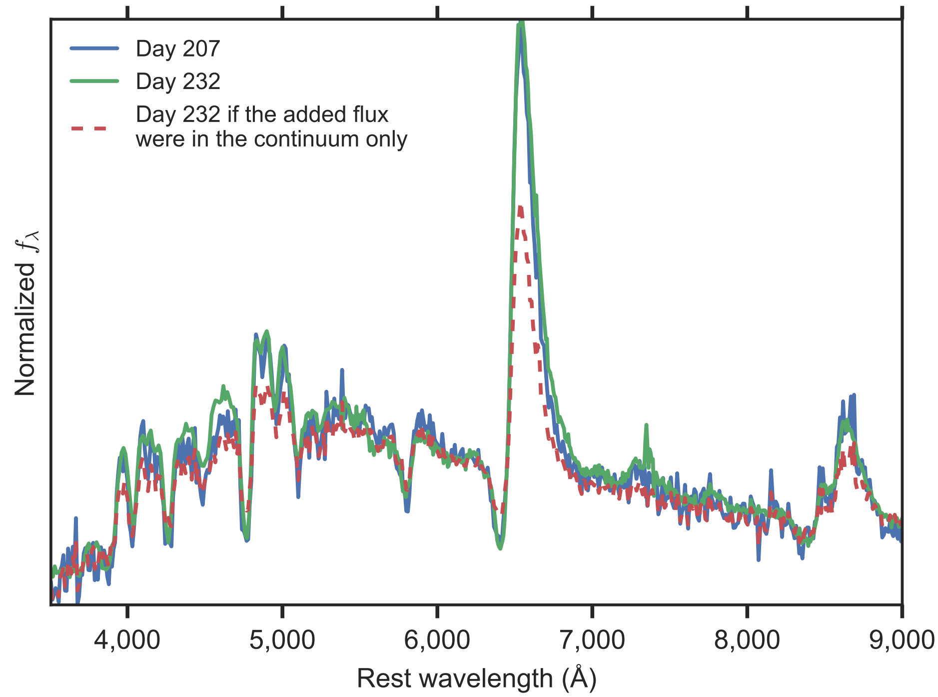

Extended Data Figure 6 Spectra of iPTF14hls expressed in terms of normalized flux density as a function of rest-frame wavelength taken on rest-frame days 207 (right before the rise to the brightest peak in the light curve) and 232 (at the brightest peak in the light curve) after discovery (solid lines). The similarity of the spectra indicate that the increase of $\approx 50\%$ in luminosity observed in the light curve between the two epochs is equal at all wavelengths. If the increase were only due to the continuum flux, then the line emission on day 232 would have been diluted in the continuum (as simulated by the dashed line).

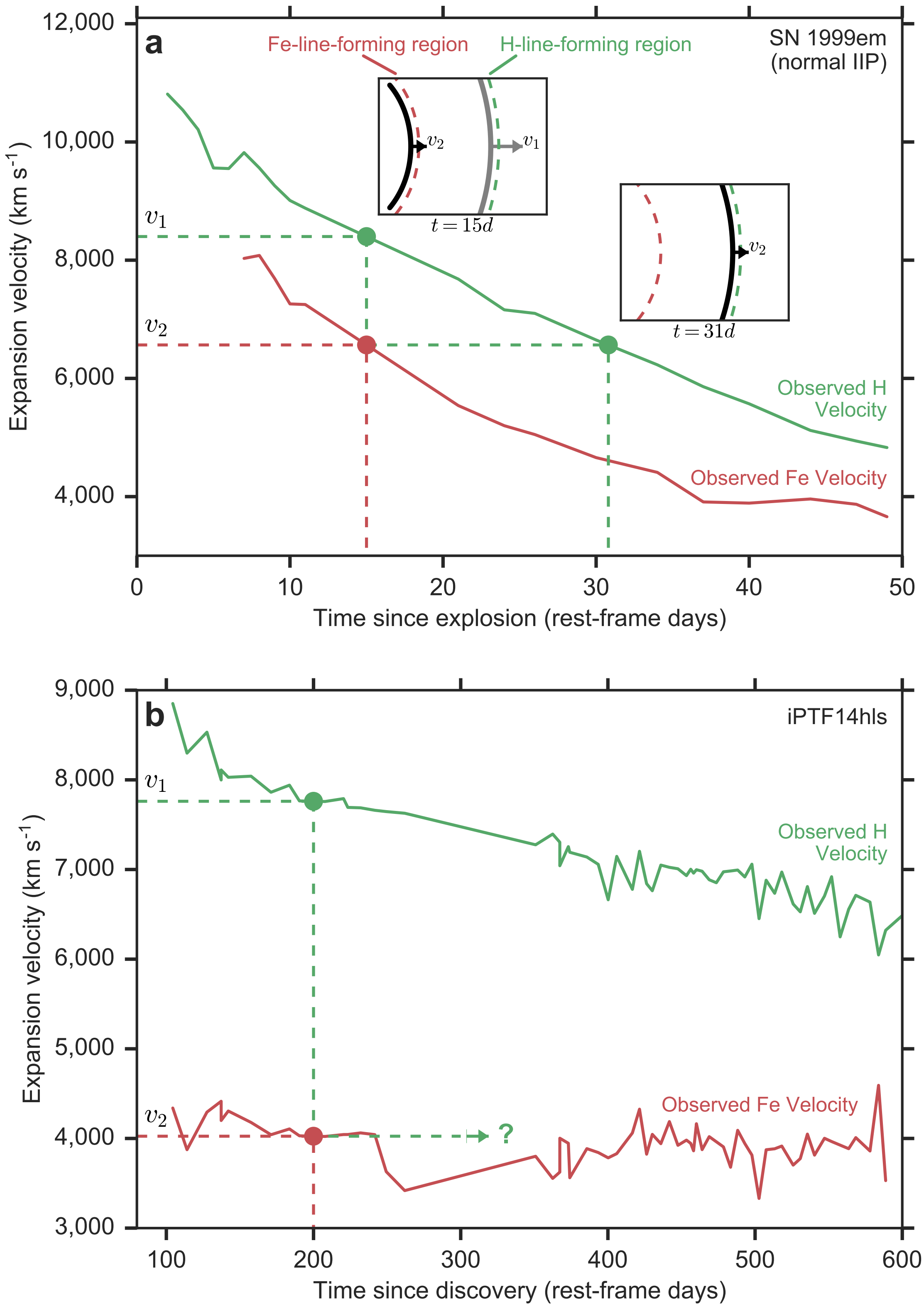

a
SN 1999em
(normal IIP)
Fe-line-forming region
H-line-forming region
v_2
v_1
$t = 15d$
$t = 31d$
Observed H
Velocity
Observed Fe Velocity
Expansion velocity (km s-1)
Time since explosion (rest-frame days)
b
iPTF14hls
?
Time since discovery (rest-frame days)

855

Extended Data Figure 7 Evolution of the measured velocity gradient in the normal Type II-P SN 1999em[22] (**a**) and in iPTF14hls (**b**). At a given time, the H-line-forming region is at material expanding with velocity v_1, while the Fe-line-forming region is at material expanding with lower velocity v_2 (top inset in panel **a**). For SN 1999em, the H-line-forming region soon reaches the material expanding at velocity v_2 as it moves inward in mass (bottom inset in panel **a**) and v_2 is measured in the H lines. For iPTF14hls, in contrast, the H-line-forming region does not reach the material expanding at v_2 even after the time since discovery increases by a factor of 6. If the material were ejected at discovery, this would indicate an increase in the radius of the line-forming regions by a factor of ≈ 6, which is unlikely given the observed velocity gradient between the H and Fe lines. If the material were ejected before discovery, on the other hand, the relative expansion in radius would be much smaller, thus offering one possible explanation for the constant velocity gradient observed in iPTF14hls.

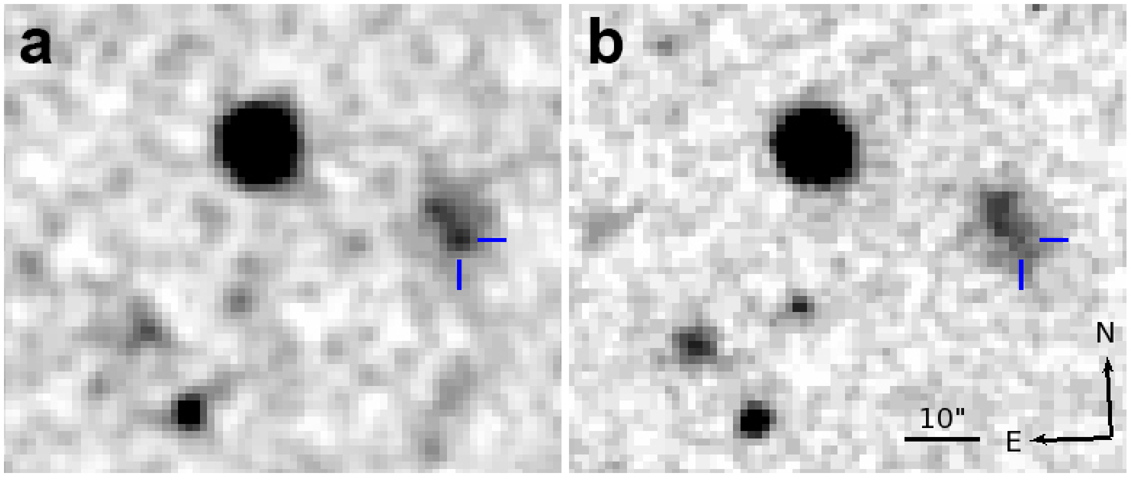

Extended Data Figure 8 Blue-filter images of of the position of iPTF14hls (marked by blue ticks) from 1954 Feb. 23 (POSS; **a**) and 1993 Jan. 2 (POSS-II; **b**). A source is visible at the position of iPTF14hls in the 1954 image, which is not there in the 1993 image. Using aperture photometry, we find that the 1954 source is $0.31{\pm}0.14$ mag brighter than the underlying host galaxy at that position, corresponding to a rough outburst magnitude of ≈ -15.6 at the luminosity distance of iPTF14hls, after removing host galaxy contribution and calibrating the field to the SDSS u+g-bands.

Line	Flux	Flux Error
[O II] 3727 Å	2.050×10^{-16}	1.152×10^{-17}
Hβ	5.666×10^{-17}	6.349×10^{-18}
[O III] 4958 Å	1.742×10^{-17}	6.130×10^{-18}
[O III] 5007 Å	1.003×10^{-16}	6.171×10^{-18}
Hα	1.539×10^{-16}	4.089×10^{-18}
[N II] 6583 Å	1.361×10^{-17}	4.095×10^{-18}

Table 1: iPTF14hls host-galaxy line fluxes (in erg $\mathrm{s}^{-1}\,\mathrm{cm}^{-2}\,\mathrm{Å}^{-1}$). Errors denote 1σ uncertainties.

Diagnostic	Metallicity	Lower Error	Upper Error
N06-N2[74]	8.339	−0.126	+0.098
N06-R23[74]	8.633	−0.166	+0.071
D02[75]	8.334	−0.166	+0.139
PP04-N2Ha[76]	8.250	−0.059	+0.044
PP04-O3N2[76]	8.309	−0.051	+0.037
M08-N2Ha[77]	8.458	−0.116	+0.076
M13-O3N2[78]	8.252	−0.035	+0.025
M13-N2[78]	8.249	−0.078	+0.060
KK04-N2Ha[79]	8.490	−0.127	+0.080
KD02comb[80]	8.386	−0.130	+0.055

Table 2: iPTF14hls host-galaxy $12 + \log$ (O/H) metallicity values under different diagnostics and calibrations. Error ranges denote 1σ uncertainties.